

國立交通大學

光電工程研究所

碩士論文

高聚焦能力多驅動電極柱狀
調變式液晶透鏡

The logo of National Central University (NCU) is a circular emblem. It features a central figure of a person holding a torch, with the year '1896' at the bottom. The emblem is surrounded by a gear-like border.

Multi-electrode Driven Cylindrical
Tunable Liquid Crystal Lens

研究生：李俊賢

指導教授：謝漢萍教授

中華民國 九十九 年 七 月

高聚焦能力多驅動電極柱狀
調變式液晶透鏡

**Multi-electrode Driven Cylindrical
Tunable Liquid Crystal Lens**

研究生：李俊賢 Student :Chun-Hsien Lee

指導教授：謝漢萍 Advisor: Dr. Han-Ping D. Shieh



國立交通大學
光電工程研究所
碩士論文

A Thesis

Submitted to Institute of Electro-Optical Engineering
College of Electrical and Computer Engineering
National Chiao Tung University

in Partial Fulfillment of the Requirements
for the Degree of Master

in

Electro-Optical Engineering

June 2010

Hsinchu, Taiwan, Republic of China

中華民國 九十九 年 七 月

高聚焦能力多驅動電極柱狀 調變式液晶透鏡

碩士研究生：李俊賢 指導教授：謝漢萍教授

國立交通大學光電工程研究所

摘 要

傳統的透鏡組由於是利用機械化的移動控制來改變透鏡間的距離，進而改變其聚焦能力，因此需要有足夠的空間來放置透鏡組。然而，在現今的照相手機市場裡，輕、薄、短、小是成為商品化的基本條件，傳統的透鏡無法滿足如此的需求，所以現今的照相手機在照相功能上是以數位變焦為主，利用數位化的技術來達到聚焦的功能，因此，其聚焦後的影像品質仍不及使用光學變焦的傳統相機。液晶透鏡具有使用電力控制即可達到光學變焦的特性，不需要額外的空間作機械式的調變，因此十分適合取代照相手機鏡頭模組中的透鏡。

本論文首先透過模擬軟體 2DimMOS 及 MatLab 建立數學模型，針對液晶透鏡上的電極圖騰設計與成像品質的關係作深入的分析討論，並提出多柱狀電極的設計來改善液晶透鏡的成像品質。接著，我們實際做出成品並與模擬結果作驗證，發現多柱狀電極因為可以分區的控制液晶轉向，因此聚焦能力遠比傳統雙電極液晶透鏡好且需要供給的電壓能量更低。在反應速度方面，我們利用提供電極短時間的高驅動電壓去幫助液晶分子的起始轉動，進而改善液晶透鏡的反應速度。此研究也更有利於將液晶透鏡應用於照相手機上。

Multi-electrode Driven Cylindrical Tunable Liquid Crystal Lens

Student: Chun-Hsien Lee

Advisor: Dr. Han-Ping D. Shieh

Department of Photonics & Institute of Electro-Optical Engineering

National Chiao Tung University

Abstract

The conventional tunable glass lenses are operated by adjusting the distance between the lenses to change the focal length. The issues of conventional tunable glass lenses are bulky and heavy. However, the compact size and light weight are very critical for the camera phone. Therefore, most of the commercial camera phones are only use the digital signal processing to simulate the zooming image, and the zooming image quality is not good enough yet. To overcome these issues, the tunable-focal lens has been developed to improve the image quality. The LC lens is electrically tunable and no moving mechanical part, which means they are compact and light weight. Therefore, the LC lens is very suitable for the application of camera phone.

In this thesis, the simulation model to characterize the feature of the LC lens with electrode pattern has been established by the commercial simulation software 2DiMOS and MATLAB. By analyzing the electrode pattern, we propose the multi-electrode driven cylindrical structure with 9 electrodes and the ratio of W_E/W_S is 1 where $W_E = W_S = 88\mu\text{m}$ to improve the focusing quality. The experiment results show the multi-electrode has smaller FWHM value of focusing performance with smaller applied voltage than the double-electrode structure. Moreover, in order to

improve the response time, large applied voltage was given to the outer large electrodes for a short time interval to help LC molecule orientation. The response time was improved by 70%. These results are helpful for applying the LC lens for the camera phone applications.



誌謝

終於完成了碩士論文，心中的感受五味雜陳。很開心的是，當初對自己碩士班這兩年的期許如今都順利的完成，心中充滿了驕傲與感謝。

首先，我要感謝我的指導教授謝漢萍老師及黃乙白老師在這兩年來對於研究上細心及嚴厲的指導及要求，並在生活上提供良好的研究環境以及傳授許多人生的哲學，老師們認真努力的研究及生活態度也深深地影響了我，未來，我也必定更加的鞭策自己努力過生活。

在研究上，首先我要感謝廖凌峯學長及林裕閔學弟給予我建議和提醒，讓我能順利完成研究。在實驗室的日子裡，感謝有鄭榮安、莊喬舜、楊柏儒、陳均合、林芳正、鄭裕國、許精益、王國振等學長們提供各方面的指導與協助。同時感謝致維、育誠、拓江、博文、宜伶、宗緯、宜如、浩彤、靖堯、佑禎、高銘、益興等同學們在課業、研究、生活上的幫助。也感謝實驗室其他學弟妹，讓實驗室充滿愉悅的氣氛。

再來我要感謝大學時代結交的好友及新竹幫，總是帶給我歡笑、活力、及勇氣，讓我對於未來充滿了的憧憬及希望。我也要感謝我的女友琬瑩，在我最沮喪及無助的時候給我支持及鼓勵，一起學習成長。最後要感謝我的父親、母親、兄長還有小白，感謝你們的栽培及照顧，你們無私的付出讓我能夠無後顧之憂的朝自己的夢想前進。最後，僅以本篇文章表達對各位的最深的謝意。

Table of Contents

Abstract(Chinese)	i
Abstract(English)	ii
Acknowledgments	iv
Table of Contents	v
Figure Caption	vii
Chapter 1	1
1.1 Camera phones	1
1.2 Tunable-focal lenses.....	2
1.2.1 Conventional tunable-focal lenses	2
1.2.2 Liquid lens	3
1.2.3 Liquid crystal lens.....	4
1.3 Motivation and Objectives.....	7
1.4 Organization of this thesis.....	9
Chapter 2	10
2.1 Principle of mechanical design on LC cell	10
2.1.1 Continuum theory	10
2.1.2 Electric field effect.....	11
2.1.3 Anchoring effect.....	13
2.1.4 Response time theory	14
2.2 Principle of optical design on LC cell.....	15
2.2.1 Optical Anisotropic of Liquid Crystal.....	15
2.2.2 Theory of Gradient Index lens	16
2.2.3 Theory of LC lens	18
2.3 Summary	19
Chapter 3	20
3.1 Fabrication technologies	20
3.1.1 ITO glass substrates rinsing	21

3.1.2 The lithography fabrication process.....	21
3.1.3 The LC device assembly process	23
3.2 Measurement System	24
3.3 Summary	24
Chapter 4	25
4.1 Introduction.....	25
4.1.1 Simulation software—2DiMOS.....	25
4.1.2 Evaluation of the lens structure.....	26
4.1.3 Application of our proposed LC lens	27
4.2 ITO electrode pattern design.....	29
4.2.1 Simulation results for double-electrode LC lens	29
4.2.2 Simulation results of multi-electrode driven structure.....	31
4.2.3 Comparison of circular and cylindrical electrode pattern.....	33
4.3 Summary	35
Chapter 5	36
5.1 Experiment results for focusing ability.....	36
5.1.1 Comparison of MeDLC and double-electrode cylindrical lens	37
5.1.2 Comparison of two combined MeDLC and single circular electrode structure lens	39
5.1.3 Combined MeDLC was used in image system	40
5.2 Experimental results for response time.....	44
5.2.1 Over-driving method: giving large applied voltage for a short time interval to help LC molecule orientation	44
5.3 Summary	49
Chapter 6	50
6.1 Conclusions.....	50
6.2 Future work.....	51

Figure Captions

Fig. 1-1 Imaging theory of the human eye.....	2
Fig. 1-2 Conventional tunable-focal lenses	3
Fig. 1-3 Structure of liquid lens: (a) no focusing state, (b) focusing state.....	3
Fig. 1-4 Structure of electro-wetting lens: (a) no focusing state (b) focusing state.....	4
Fig. 1-5 Operation mechanism of the inhomogeneous LC distribution structure.....	6
Fig. 1-6 Operation mechanism of monomer and LC mixed structure (a) voltage-off state, (b) voltage-on state, (c) side-view of the whole structure in the voltage-on state	6
Fig. 1-7 Operation mechanism of the homogeneous electric field structure (a) side-view and (b) top-view	7
Fig. 2-1 The equilibrium configuration of nematic liquid crystals	11
Fig. 2-2 The schematic relationship between LC and electric field.....	12
Fig. 2-3 Different alignment arrangements of upper and lower substrates in (a) TN, (b) anti-parallel rubbing, and (c) pi-cell	13
Fig. 2-4 The mechanism of GRIN lens	16
Fig. 2-5 The ideal parabolic curve function of Δn and radius	18
Fig. 2-6 The mechanism of GRIN LC lens	19
Fig. 3-1 Flow chart of LC lens fabrication	20
Fig. 3-2 Flow chart of substrate rinsing process	21

Fig. 3-3 Flow chart of lithography process	22
Fig. 3-4 Flow chart of the LC device assembly process	23
Fig. 3-5 Schematic diagram of the measurement system	24
Fig. 4-1 The graphical user interface of 2DiMOS	26
Fig. 4-2 The configuration of our proposed LC lens	28
Fig. 4-3 The distribution of Δn of double-electrode structure	30
Fig. 4-4 Flow chart of the simulation steps.....	31
Fig. 4-5 Simulation result of error function with electrode number	32
Fig. 4-6 Simulation result of error function with Ratio of WE/WS.....	32
Fig. 4-7 Simulation result of MeDLC structure.....	32
Fig. 4-8 Top view of the multi-electrode circular pattern structure	33
Fig. 4-9 Multi-ring electrode layers structure (a) Side-view and (b) Top-view.....	33
Fig. 4-10 Mechanism of multi-electrode cylindrical LC lens.....	34
Fig. 4-11 Schematic diagram of the combination of two cylindrical LC lens	34
Fig. 4-12 The schematic of various polarizations	35
Fig. 4-13 Flow chart of simulation steps for new specification design	35
Fig. 5-1 The multi-electrode driven cylindrical LC lens sample (MeDLC)	36
Fig. 5-2 The diagram of FWHM.....	37
Fig. 5-3 Experiment results for distribution of intensity which the focal length was	

fixed at 4cm : (a) MeDLC and (b) double-electrode cylindrical structure	38
Fig. 5-4 Photo of experimental system of combined MeDLC.....	39
Fig. 5-5 Experimental results for distribution of intensity :	40
Fig. 5-6 The image results in FPGA : (a) LC lens without applied voltage	41
Fig. 5-7 The combined MeDLC may generate serious optical aberration.....	41
Fig. 5-8 The calculation of MTF by convoluting the rectangle wave and beam profile	42
Fig. 5-9 The calculating results of MTF by the beam profile : (a) the experimental result of beam profile, (b) the modified result of beam profile and(c) the comparison of MTF in different beam profile	43
Fig. 5-10 Experimental results of MeDLC on intensity value as a function of time...	45
Fig. 5-11 Two larger electrodes were added outside the original 9 electrodes	46
Fig. 5-12 The voltage control system in over-driving method.....	46
Fig. 5-13 Experimental result for the Δt with different applied voltage of the outer large electrodes (V_L).....	47
Fig. 5-14 The experimental result for the applied voltage on 80Vrms of intensity value as a function of time.....	47
Fig. 5-15 Too large applied voltage will induce large Δt value	48
Fig. 5-16 The experimental results for distribution of intensity at $V_L=80Vrms$ and $\Delta t=4s$, (a) distribution of intensity gray level and (b) intensity value as a function of time	49

Fig. 6-1 The concept of combining electrodes with high resistance layer, (a) side-view and (b) equivalent circuit of high resistance layer52

Fig. 6-2 Cylindrical structure will induce rectangle equivalent voltage line.52

Fig. 6-3 The schematic of dot array electrodes with high R material structure52

List of Tables

Table 1. The specification of current camera phone lens.....28

Table 2 The parameters for our proposed LC lens.....29



Chapter 1

Introduction

1.1 Camera phones

In recent years, there has been a dramatic revolution research focusing on mobile phones. More than the communication function, there are many supplementary functions such as: surfing the internet, listening to the music, playing the video game and taking photograph, etc. According to the report from Institute for Information Industrial, the mobile phones began to have the taking photograph function since 2001, and the popularity of the function has become more than 70% at present. On the other hand, the image resolution taken by camera phone has also progressed tremendously from 110 thousands to more than 5 millions. With the increasing usage of the camera phone, the requirements for the optical focusing system have become more critical. In addition to basic image quality, the required properties of image system of mobile phones including thin format, compact size, light weight, and low power consumption. Thus, current tunable-focal lens module is not suitable for the camera phone and most of the commercial camera phones are only used the digital signal process to simulate to real image. However, the zooming image quality with only the digital signal process is not good enough. Therefore, there are several technologies have been developed in order to meet the requirements which has mentioned above. In this thesis, most effort will be devoted on developing a high image quality tunable-focal lens to improve the image quality in the camera phone.

1.2 Tunable-focal lenses

Tunable-focus lenses already exist in the nature. For instance, the human eye is a single-lens system with tremendously wide tunable focus range. The primary tuning mechanism is shape change, as controlled by the muscles in the eye, as shown in Fig. 1-1. As the incident light passing by the lens, it will focus on the retina, and the retina creates an image signal of the visual world for the brain. In order to mimic this characteristic, there are some practical methods reported, including conventional tunable-focal lenses, liquid lens, and liquid crystal lens, described in the following section.

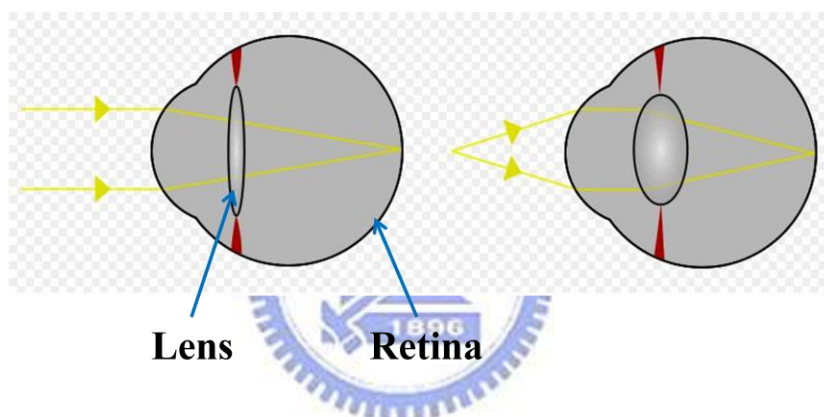


Fig. 1-1 Imaging theory of the human eye

1.2.1 Conventional tunable-focal lenses

The conventional tunable-focal lenses are composed of several pieces of individual lens, and most of the conventional lenses are made of glass or other transparent material. These lenses can reconfigure the transmitted light beam. Adjusting the distance (d) between the lenses by mechanical movement varies the focal length [1], as shown in Fig. 1-2. However, it needs some volume to let the lenses adjusting which can accomplish the tunable-focal function. Therefore, the issues of this structure are bulky and heavy. As the small size and light weight requirements increase, the other technologies have been developed.

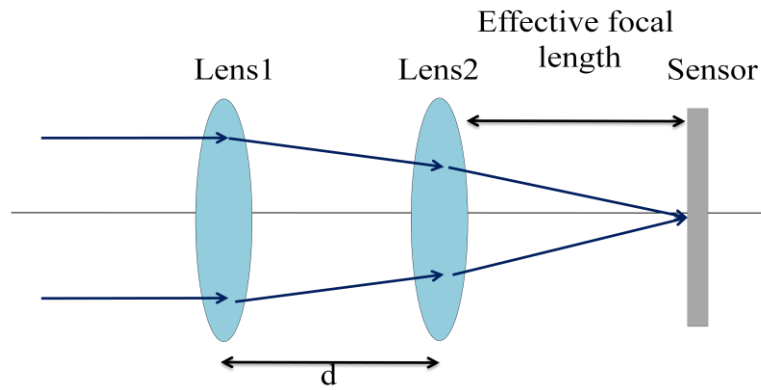


Fig. 1-2 Conventional tunable-focal lenses

1.2.2 Liquid lens

Similar to the glass lens, a liquid lens focuses the incident light based on the changing of surface profile. According to the operation method, liquid lenses can be classified into two types. The first type is mechanical lens which the focal length is controlled by pumping liquid. The second type is electro-wetting lens which the focal length is controlled by applying different external voltage.

1.2.2.1 Mechanical liquid lens technology

This kind of liquid lens is filled with only one kind of fluid and sealed with the elastic membrane. Pumping liquid in the chamber which changes the curvature of the liquid profile can create different focal length, as shown in Fig. 1-3 [2]

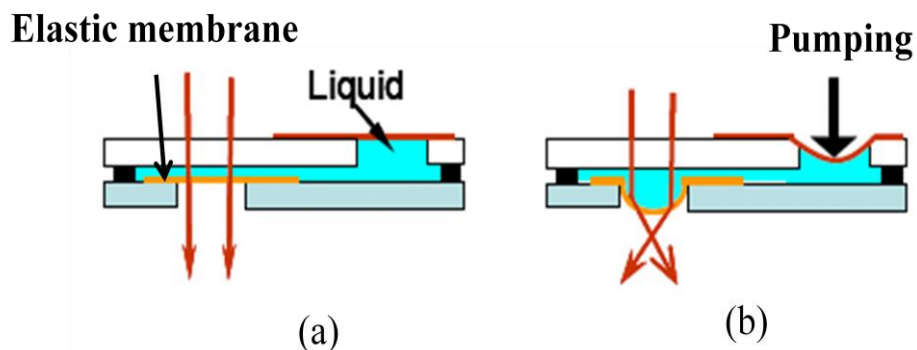


Fig. 1-3 Structure of liquid lens: (a) no focusing state, (b) focusing state

1.2.2.2 Electro-wetting liquid lens technology

Electro-wetting liquid lens is filled with two different kinds of fluid substrates, such as water and oil which have different density, dielectric constant and viscosity. The voltage applied to the substrate can induce different electrical force to vary the curvature of fluids profile which leads to different focal length, as shown in Fig. 1-4 [3].

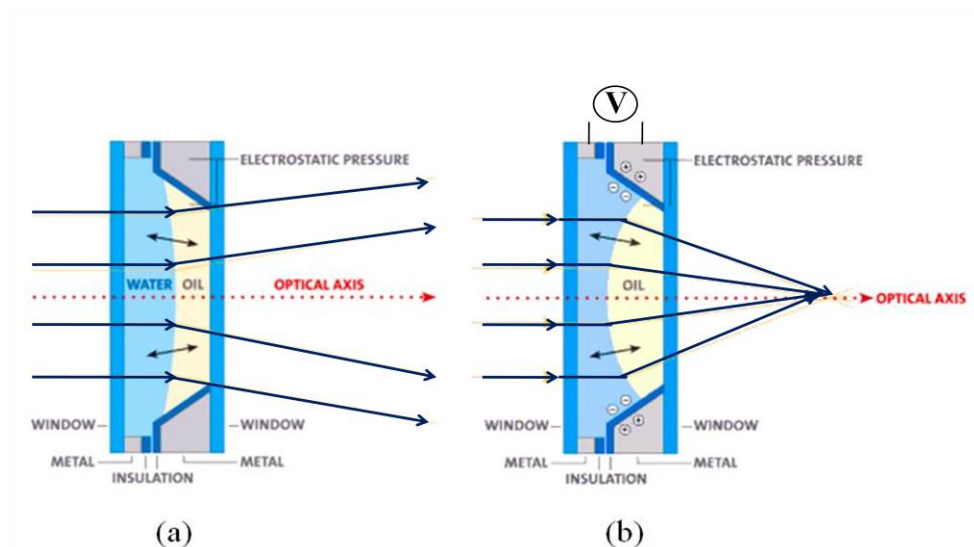


Fig. 1-4 Structure of electro-wetting lens: (a) no focusing state (b) focusing state

1.2.3 Liquid crystal lens

In the last decade, many advances have been made in the area of Liquid crystal materials which have been widely used for the display and other electro-optic devices due to their physical properties such as birefringence and effect by the electric field. The way of applied voltage which can generate non-uniform electric field distribution will vary the liquid crystal director, which denote the optical phase and path will be changed.

A number of studies have investigated the LC lens which can be traced back to

1979, a paper was published by Susumu Sato that has been the subject of much discussion ever since.[4] The structure could change the focal length by adjusting the applied voltage. The suitable liquid crystal distribution can generate and control the optical path difference between the center and the edge of the cell. The optical function could be the same to the convex or concave lens. Since the electric field distribution is very essential for the liquid crystal director, how to design the electrode structure and applying the voltage to form appropriate electric field distribution has been the subject of active research. The liquid crystal lens can be classified into: inhomogeneous and homogeneous electric field approaches. Following the approach and characteristic of each type will be introduced.

1.2.3.1 Inhomogeneous electric field approaches

Inhomogeneous liquid crystal distribution

In order to generate a inhomogeneous electric field, the structure need to deposit the indium-tin-oxide (ITO) electrode on a concave substrate, as shown in Fig. 1-5 [4]. In the voltage-off state, the effective refractive index of liquid crystal is n_e , which the incident light can be focused. In the voltage-on state, the inhomogeneous electric field reorients the liquid crystal and the effective refractive index become n_o , which have long focal length. The advantages of this structure are: lower operation voltage and shorter initial focal length. However, the issue of this structure is higher optical aberration.

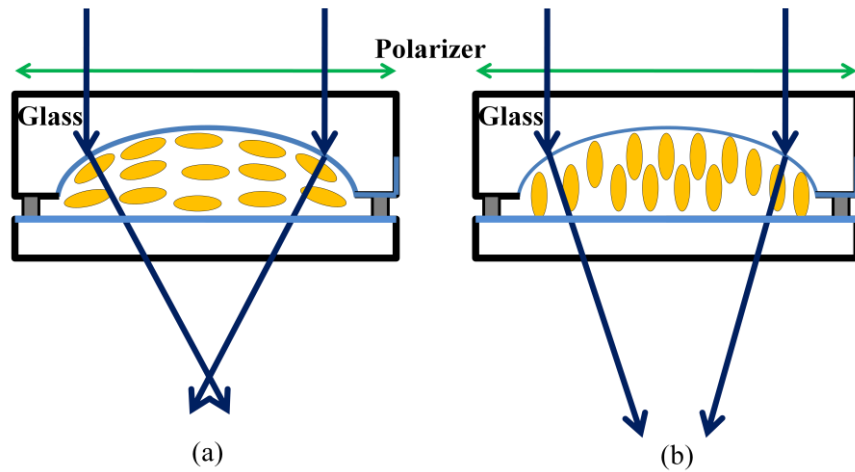


Fig. 1-5 Operation mechanism of the inhomogeneous LC distribution structure

(a) Voltage-off and (b) Voltage-on state

Monomer and liquid crystal mixed

By applying the inhomogeneous electric field, an adaptive lens using electrically induced LC and monomer, which have different refractive indexes, concentration redistribution was proposed [5]. The electric field makes the LC molecules to diffuse towards the high electric field region and the liquid monomer towards the lower electric field region, as shown in Fig. 1-6. An inhomogeneous electric field can generate the non-uniform distribution of LC and monomer, as shown in Fig. 1-6 (c). Therefore, a gradient refractive index lens has been obtained. The advantage of this structure is lower optical aberration, but its response time is slow.

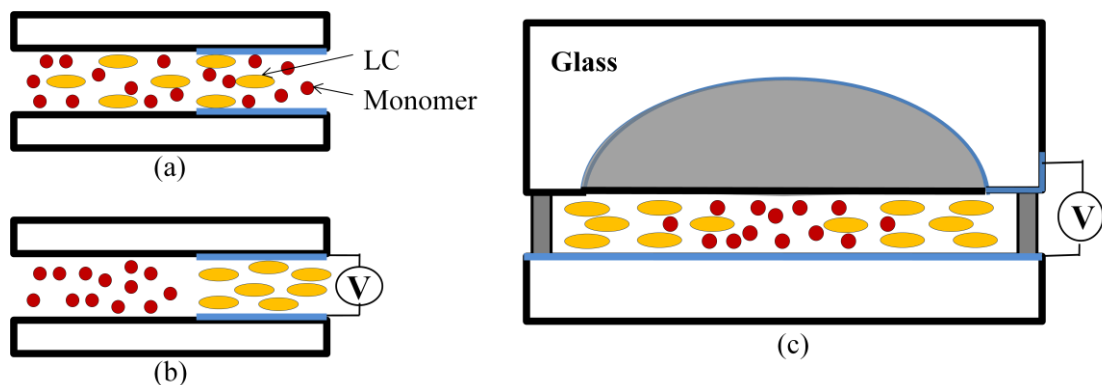


Fig. 1-6 Operation mechanism of monomer and LC mixed structure (a) voltage-off state, (b) voltage-on state, (c) side-view of the whole structure in the voltage-on state

1.2.3.2 Homogeneous electric field approaches

The other kind of liquid crystal lens is controlling the LC director distribution by designed electrode shape, as shown in Fig. 1-7. Applying different voltages to the outer and inner electrodes can generate a spatial non-uniform and symmetrical electric field in the LC layer. It can also behave as convex or concave lens by controlling the applied voltage. For instance, applying voltage V_1 higher than the voltage V_2 , the LC director in the outer position will follow the electric field direction perpendicular to the electrode, and the incident polarized light beam will see n_o which is smaller than n_e . Therefore, the LC lens has a gradient refractive index distribution and behaves as conventional convex lens. However, the most critical issue of this structure is the LC director will disorder at the connecting electrode position, and generate a poor image quality.

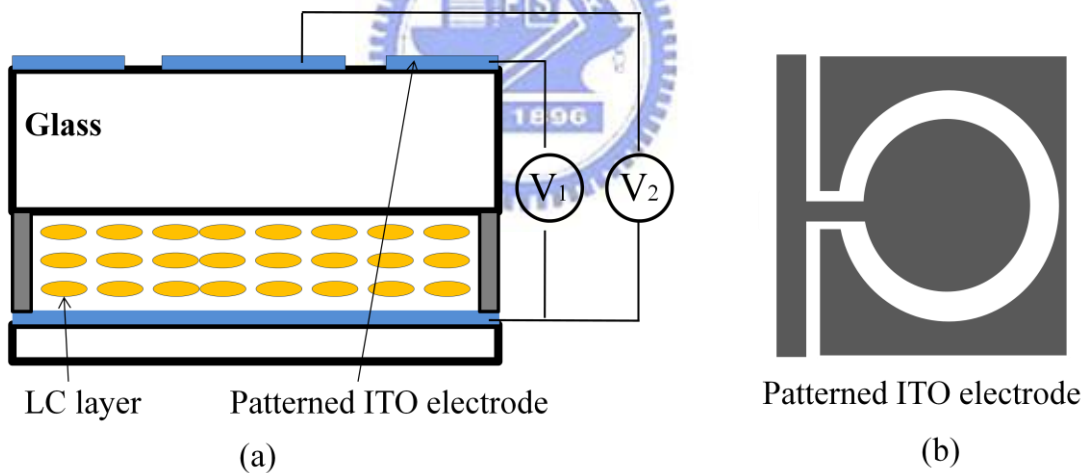


Fig. 1-7 Operation mechanism of the homogeneous electric field structure (a) side-view and (b) top-view

1.3 Motivation and Objectives

With the increasing usage of camera phone, the requirements for the auto-focusing (AF) and zooming function have become more critical. However, the conventional

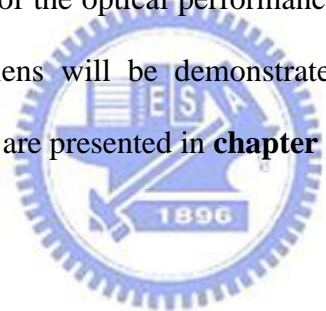
approaches are composed of several pieces of glass lenses, and take the mechanical movement of individual lenses to accomplish the necessary functions. Therefore, the conventional lens module would be much thicker and heavier. Based on the reasons mentioned above, most of the commercial camera phones are only use the digital tunable lens to simulate the real image, and the zooming image quality would not good enough. To overcome these issues, there are several approaches have been presented. This thesis is focus on the LC lens.

The LC lens has unique properties such as electrically tunable focal length. Since there are no moving mechanical parts, the LC lens can smaller and lighter than the conventional tunable glass lenses. As the requirement, if the LC lens could replace the conventional lenses, it would not only reduce the thickness and weight, but also have the optical tunable-focal function which can combine with digital tunable-focal lens to generate higher image quality.

There are a number of studies that have investigated how to achieve better optical performance by the LC lens by designing the electrodes and arrangement of applied voltage value to form an appropriate distribution of non-uniform electric field. The objective in this thesis is to design the pattern of ITO electrode to generate a high optical performance LC lens. By evaluating the issue of conventional circle driven electrodes, the disordered LC director at the connecting electrode position is inevitable. Therefore, we propose a multi-electrically driven cylindrical LC lens (MeDLC) which can yield a desired gradient refractive index profile over the whole LC layer. By adjusting the driving voltage, an LC lens with higher optical performance can be generated.

1.4 Organization of this thesis

This thesis is organized as follows: in **chapter 2**, basic principles and theories used in this thesis will be introduced. The principles of mechanical design on the LC cells including the continuum theory, anchoring effect, and response time are described, and the principles of optical design on the LC Cell including the physical property of LC material, GRIN lens and LC lens are also presented. In **chapter 3**, the fabrication technologies to realize our liquid crystal lens are summarized. The measurement equipments will be illustrated. In **chapter 4**, the simulation results of the multi-electrically driven liquid crystal (MeDLC) lens will be reported, where the merit of this structure is high optical performance. A mathematical model has been developed for the evaluation of the optical performance of the LC lens. In **chapter 5**, the realization of MeDLC lens will be demonstrated and discussed. Finally, the conclusions and future works are presented in **chapter 6**.



Chapter 2

Theory and Principle

The mechanical and optical designs of the LC lens are introduced in this chapter. In the principle of mechanical design, the continuum theory is used to calculate the Gibbs's energy of the certain state, the anchoring effect is used to calculate the alignment effect on the orientation of LC director, and the response time equation is used to describe the parameters which can affect the response time of the LC cell. In the principle of optical design, the gradient index lens and the optical anisotropic effect of LC are used to generate non-uniform refractive index lens, and the basic action theory of LC lens will be introduced.

2.1 Principle of mechanical design on LC cell

The switching performance of the LC device relies on its mechanical design. In order to realize the principle of the liquid crystal, some properties and advantages will be introduced.

2.1.1 Continuum theory

Frank-Oseen continuum theory is widely used to calculate the equilibrium profile of LC directors in the cell. [6][7][8] This theory can be explained by Eq. 2-1, where \mathbf{n} is the vector of LC director, \mathbf{q}_0 is $\frac{2\pi}{p}$ which p denotes pitch of liquid crystal helix, and K_{11} , K_{22} and K_{33} are the elastic constants of splay, twist, and bend state, respectively, as shown in Fig. 2-1. After applying the voltage, the nematic type of LC have deformation phenomenon.

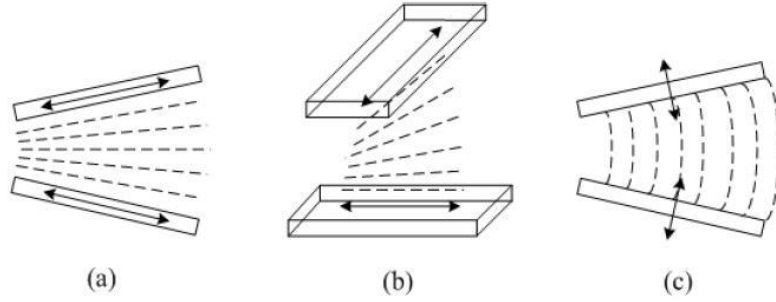


Fig. 2-1 The equilibrium configuration of nematic liquid crystals

(a) splay, (b) twist, and (c) bend motions

$$F = \frac{1}{2} \{ K_{11} (\nabla \cdot \mathbf{n})^2 + K_{22} [\mathbf{n} \cdot (\nabla \times \mathbf{n}) - q_0]^2 + K_{33} [\mathbf{n} \times (\nabla \times \mathbf{n})]^2 \} - \frac{1}{2} (\mathbf{D} \cdot \mathbf{E}) \quad (2-1)$$

$$\text{and } \mathbf{n} = \begin{bmatrix} n_x \\ n_y \\ n_z \end{bmatrix}$$

where F is the free energy function which conform to the elastic continuum theory of liquid crystals.



2.1.2 Electric field effect

In this thesis, we only consider the nematic LC which is uniaxial material. There are two dielectric constants for the rod-like LC director, as shown in Fig. 2-2. One is the dielectric constant ϵ_{\parallel} which is measured under the electric field parallel to the long axis of the LC director. The other is the dielectric constant ϵ_{\perp} which is measured under the electric field perpendicular to the long axis of the LC director. The dielectric anisotropy is defined as $\Delta\epsilon = \epsilon_{\parallel} - \epsilon_{\perp}$. When the electric field is applied to the LC, the electric displacement \vec{D} can be described as Eq.2-2.

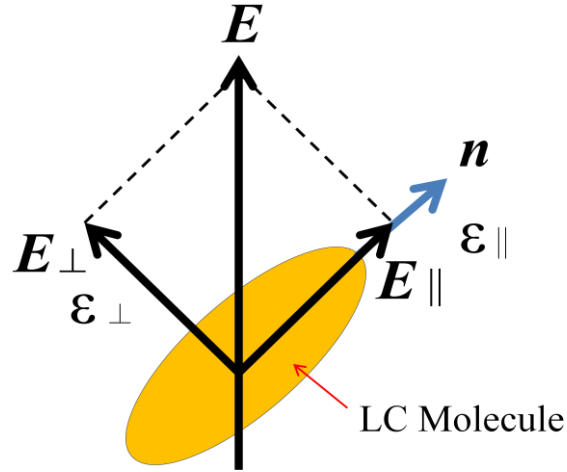


Fig. 2-2 The schematic relationship between LC and electric field

$$\begin{aligned}
 \vec{D} &= \vec{D}_{\parallel} - \vec{D}_{\perp} \\
 &= \epsilon_0 \epsilon_{\parallel} (\vec{E} \cdot \vec{n}) \vec{n} + \epsilon_0 \epsilon_{\perp} [\vec{E} - (\vec{E} \cdot \vec{n}) \vec{n}] \\
 &= \epsilon_0 [\epsilon_{\perp} \vec{E} + \epsilon_{\parallel} (\vec{E} \cdot \vec{n}) \vec{n} - \epsilon_{\perp} (\vec{E} \cdot \vec{n}) \cdot \vec{n}] \\
 &= \epsilon_0 [\epsilon_{\perp} \vec{E} + (\epsilon_{\parallel} - \epsilon_{\perp}) (\vec{E} \cdot \vec{n}) \cdot \vec{n}] \\
 &= \epsilon_0 [\epsilon_{\perp} \vec{E} + \Delta\epsilon (\vec{E} \cdot \vec{n}) \cdot \vec{n}] \tag{2-2}
 \end{aligned}$$

where the \vec{E} denotes applied electric field.

The electric free energy of the system (F_{elec}) can be described by Eq. 2-3.

$$\begin{aligned}
 F_{\text{elec}} &= -\frac{1}{2} \vec{E} \cdot \vec{D} \\
 &= -\frac{1}{2} \epsilon_0 \epsilon_{\perp} E^2 - \frac{1}{2} \epsilon_0 \Delta\epsilon (\vec{E} \cdot \vec{n})^2 \tag{2-3}
 \end{aligned}$$

The first term is no concerned with the LC director orientation, and it can be supposed to be a constant value for the energy of the system and can be neglected. In considering the second term which is directly concerned with LC director orientation, the positive type nematic LC ($\Delta\epsilon > 0$) will follow the applied electric field direction to remain the electric free energy and free energy in the lowest state.

2.1.3 Anchoring effect

The LC alignment affects the equilibrium state and director configuration of the LC cell. The alignment is generally achieved by the anchoring effect with a pretreated layer, and polyimide is used owing to its low cost, high stability, and easy process. Two major methods are used to pre-treat the alignment material: mechanical rubbing and photo-alignment, and the mechanical rubbing method have been used in our fabrication. The method is executed by a roller covered with woolen texture. By brushing in the same direction, the alignment will strain the LC director to the certain direction. By varying the alignment directions of the upper and lower substrates, the cell can be stabilized into different LC profile, as shown in Fig. 2-3. The 90°, anti-parallel, and parallel alignments can produce the twist nematic(TN), electrically controlled birefringence, and pi-cell, respectively.[9]

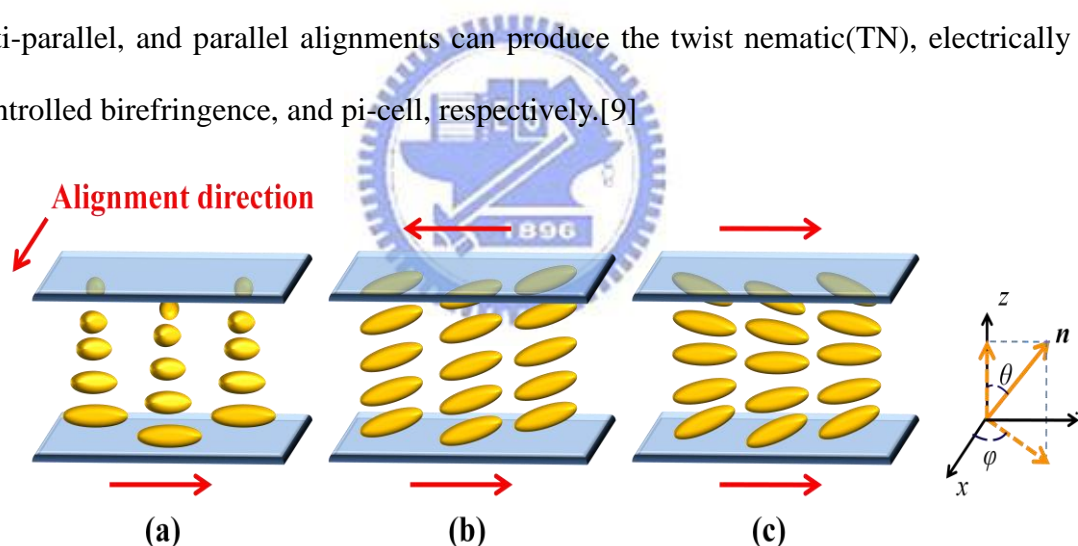


Fig. 2-3 Different alignment arrangements of upper and lower substrates in (a) TN, (b) anti-parallel rubbing, and (c) pi-cell

The mechanism for stabilizing the free energy can be expressed by Rapini-Papoular approach [10][11] [12] as follows:

$$F_s = F_\theta + F_\phi \quad (2-4)$$

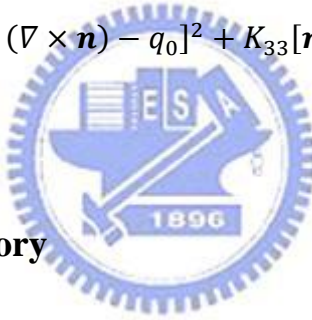
$$F_\theta = \frac{1}{2} W_\theta \sin^2(\theta - \theta_0) \quad (2-5)$$

$$F_\varphi = \frac{1}{2}W_\varphi \sin^2(\varphi - \varphi_0) \quad (2-6)$$

where θ and φ denote the polar and azimuthal angles, F_s denotes the total free energy resulting from the anchoring effect, F_θ denotes the free energy component in terms of the polar angle, F_φ denotes the free energy component in terms of the azimuthal angle. W_θ and W_φ are the constants whose physical meanings are the interactions between the substrates and the LC director. θ_0 and φ_0 are the equilibrium angles in the polar and azimuthal dimensions, respectively.

By considering the anchoring effect, the continuum equation can be modified as Eq. 2-7, and this equation can be used to describe the stabilized LC director profile of the LC cell.

$$F = \frac{1}{2}\{K_{11}(\nabla \cdot \mathbf{n})^2 + K_{22}[\mathbf{n} \cdot (\nabla \times \mathbf{n}) - q_0]^2 + K_{33}[\mathbf{n} \times (\nabla \times \mathbf{n})]^2\} - \frac{1}{2}(\mathbf{D} \cdot \mathbf{E}) + F_s \quad (2-7)$$



2.1.4 Response time theory

For the LCD technology, switching between different gray levels determines the real response time. By the Erickson-Leslie equation, ignored the twist elastic constant (K_{22})、backflow effect and inertia effect, the dynamic response time can be described in Eq. 2-8 , where the E denotes the applied voltage, and γ_1 denotes the rotational viscosity. [13][14]

$$(K_{11}\cos^2\theta + K_{33}\sin^2\theta)\frac{\partial^2\theta}{\partial Z^2} + (K_{33} - K_{11})\sin\theta\cos\theta\left(\frac{\partial\theta}{\partial Z}\right)^2 + \varepsilon_0\Delta\epsilon E^2\sin\theta\cos\theta = \gamma_1\frac{\partial\theta}{\partial t} \quad (2-8)$$

From the small angle approximation, the rise and decay response times of the LC cell can be described in Eqs.2-9 and 2-10, where d denotes LC cell gap, K denotes elastic constant, V_{th} denotes threshold voltage, V_b denotes bias voltage, and V denotes

applied voltage.

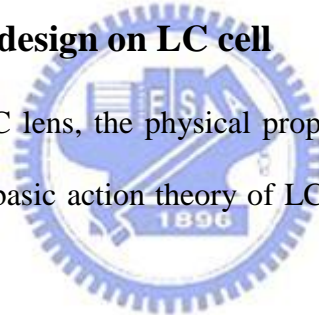
$$\tau_{rise} = \frac{\gamma_1 d^2 / K \pi^2}{(V/V_{th})^2 - 1} \quad (2-9)$$

$$\tau_{decay} = \frac{\gamma_1 d^2 / K \pi^2}{|(V_b/V_{th})^2 - 1|} \quad (2-10)$$

From the equation, the response time is proportional to the $1/d^2$ and $1/V^2$. No doubt, the thicker the LC layer, the slower the response time. On the other hand, the over-drive method has been popular used in the LCD technology. This method is over applying the drive-voltage to accelerate the LC rotate response, and adjusting the applied voltage to the appropriate voltage. Therefore, it can reduce the LC response time.

2.2 Principle of optical design on LC cell

In the optical design of LC lens, the physical properties of liquid crystal, and the gradient index lens, and the basic action theory of LC lens will be introduced in this section.



2.2.1 Optical Anisotropic of Liquid Crystal

There are several kind of liquid crystal material such as biaxial material, uniaxial material, positive type, and negative type. In this thesis, the Merck E7 LC material has been used to experiment which is positive type and uniaxial nematic material. The nematic liquid crystal material has the birefringence property including ordinary refractive index and extraordinary refractive index. The incident light beam will see the ordinary refractive index when the polarization of the light perpendicular to the optical axis. On the other hand, the incident light beam will see the extraordinary refractive index when the polarization of the light parallel to the optical axis. The

effective refractive index can be calculated in Eq.2-11.

$$n_{eff}(\theta) = \frac{n_o n_e}{\sqrt{n_e^2 \sin^2 \theta + n_o^2 \cos^2 \theta}} \quad (2-11)$$

where the θ denotes the angle between the polarization of incident light and LC optical axis, and the n_e and n_o denote the refractive index for the ordinary light beam and the extraordinary light beam, respectively.

2.2.2 Theory of Gradient Index lens

The most important rule of the lens is the incident planar wavefront should pass the same optical path. As the incident light passing the refractive index medium, the passing velocity can be described in the equation $v = c/n$, where the c , n , and v are the velocity in the vacuum, index of refraction and velocity in the medium. The light beam has higher speed while passing by the lower refractive index medium. The refractive index of the lens which is gradient distributing has been called gradient refractive index (GRIN) lens. Therefore, the incident light beam passing by the GRIN lens would focus on the focal point, as shown in Fig. 2-4.

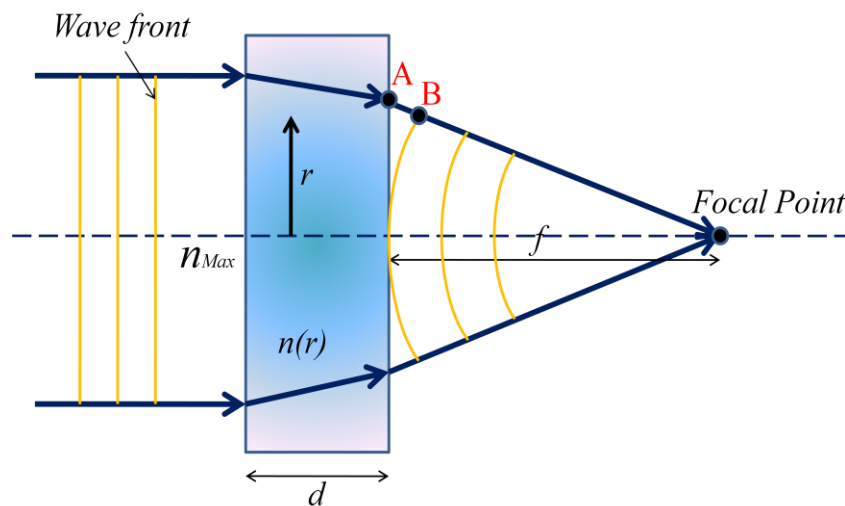


Fig. 2-4 The mechanism of GRIN lens

where the n_{Max} denotes the refractive index in the center which has the maximum value, the $n(r)$ denotes the refractive index varied by the radius position, f denotes the focal length of the lens. Since the planar wavefront has been bended into a spherical wavefront, the optical path between the center and edge of the cell can be expressed as:

$$\begin{aligned} n(r)d + AB &= n_{Max}d \\ \Rightarrow AB &= [n_{Max} - n(r)]d \end{aligned} \quad (2-12)$$

Furthermore, the geometry parameter can be expressed as:

$$\begin{aligned} AB &= AF - f \\ AF &= \sqrt{r^2 + f^2} \end{aligned} \quad (2-13)$$

Therefore, the optical path can be expressed as:

$$\begin{aligned} [n_{Max} - n(r)]d + f &= \sqrt{r^2 + f^2} \\ \Rightarrow n_{Max} - n(r) &= \frac{\sqrt{r^2 + f^2} - f}{d} \end{aligned} \quad (2-14)$$

Because the focal length value (f) is much higher than lens radius value (r), the Fresnel' approximation [15] can be used as follows:

$$\begin{aligned} \sqrt{r^2 + f^2} &\approx f \left[1 + \frac{1}{2} \left(\frac{r}{f} \right)^2 \right] \\ \Rightarrow n(r) &= n_{Max} - \frac{f \left[1 + \frac{1}{2} \left(\frac{r}{f} \right)^2 \right] - f}{d} \\ &= n_{Max} - \frac{r^2}{2fd} \\ \Rightarrow f &= \frac{r^2}{2d[n_{Max} - n(r)]} = \frac{r^2}{2d \cdot \Delta n} \end{aligned} \quad (2-15).$$

where Δn denotes the refractive index difference between the center and edge of the cell. The focal length formula has been obtained in Eq.2-15, the focal length is varied by the thickness of the lens (d) and the refractive index difference (Δn) between the

lens center and edge of the cell.

By the transposition of Eq.2-15, another represent of Δn can be expressed as shown in Eq.2-16.

$$\Delta n = \frac{r^2}{2d_{LC}f} = \kappa r^2 \quad (2-16)$$

Every position of the ideal lens should have the same focal length or the lens will have optical aberration. Thus, the Δn is a function of parabolic curve with r^2 , where $\kappa = 1/2d_{LC}f$ is a constant. Therefore, the ideal relationship between the Δn and r^2 is a smooth parabolic curve function, as shown in Fig. 2-5.

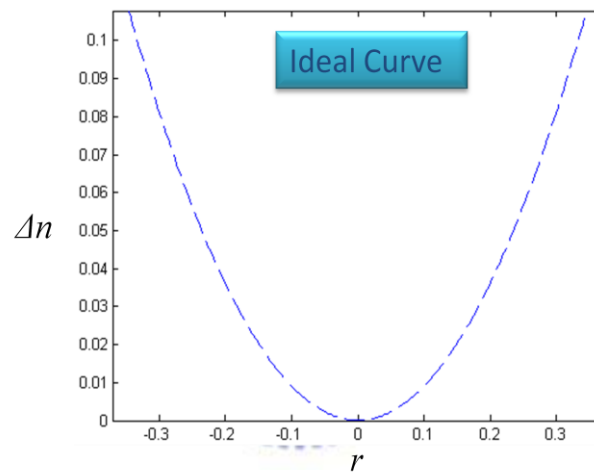


Fig. 2-5 The ideal parabolic curve function of Δn and radius

2.2.3 Theory of LC lens

Liquid crystal materials have been widely used for the display and other electro-optic devices due to their physical properties such as birefringence and effect by the electric field. Tuning the voltage applying way which can generate no-uniform electric field distribution will change the liquid crystal director. Therefore, the GRIN LC lens will be generated, as shown in Fig. 2-6. At first, the incident light beam has to pass the polarizer. Then, the polarized incident light will see the effective refractive

index while passing the LC layer, and vary the light beam direction. The focusing theory is described in Eq. 2-15.

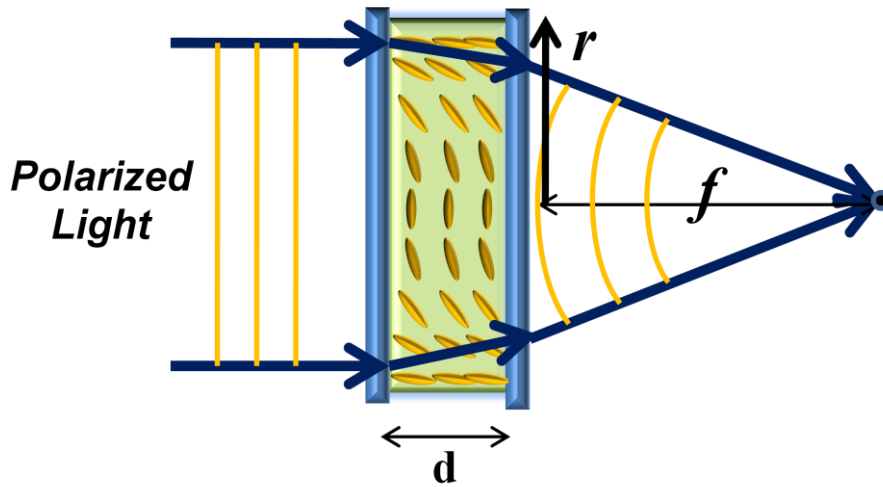


Fig. 2-6 The mechanism of GRIN LC lens

2.3 Summary

The principles of mechanical and optical designs of the LC lens are introduced in this chapter. In mechanical design, the continuum theory is used to calculate the Gibbs's energy of the certain state, the anchoring effect is used to calculate the alignment effect on the orientation of LC director, and the response time equation is used to describe the parameters which can affect the response time of the LC cell. In optical design, the gradient index lens and the optical anisotropic effect of LC are used to generate non-uniform refractive index lens, and the basic action theory of LC lens has been introduced. The results which were discussed in chapters 4 and 5 are all basic on these principles.

Chapter 3

Device fabrication and measurements

The basic fabrication processes and measurement methods of LC lens are described. These fabrication steps will be used to realize our designed devices. After the devices being fabricated, the characterization of the optical performance is measured with the beam profile CCD sensor.

3.1 Fabrication technologies

The basic fabrication processes is as shown in Fig. 3-1. First of all, the ITO glass substrates are cut into suitable size. Secondly, the ITO glass substrates are rinse which is very important for the following steps. Thirdly, the lithography fabrication processes including spin coating, photomask generating, UV light exposing and development will be used. Finally, the assembly processes including the polyimide (PI) coating and rubbing, spacer pasting, LC injecting, cell sealing and external circuits connecting will be described in the follow.

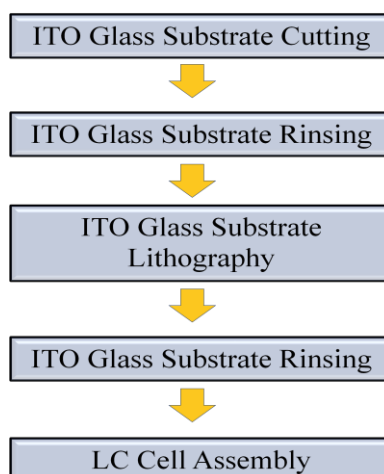


Fig. 3-1 Flow chart of LC lens fabrication

3.1.1 ITO glass substrates rinsing

ITO glass substrates rinsing is very crucial for the following steps. Wet rinsing processes are necessary to obtain an ultra clean the surface for the subsequent fabrication. Cleaning removes particles and chemical impurities from the surface without damaging or altering the substrate surface. The flow chart of this rinsing process is as shown in Fig. 3-2. First of all, the Acetone has been used to rinse the glass which can clean the organic leftover on the substrate. The Acetone can also clean the photoresist. Secondly, the detergent has been used by the hands to wash the substrate. Because the ITO and glass substrates are the hydrophilic material, the substrate is clear or not can be checked by the water distribution. The sprayed water on the substrate uniformly distributed implies that the substrate is clean. Thirdly, the de-ionized (DI) water is used to clean the substrate. Finally, the heater is used to evaporate the left water.

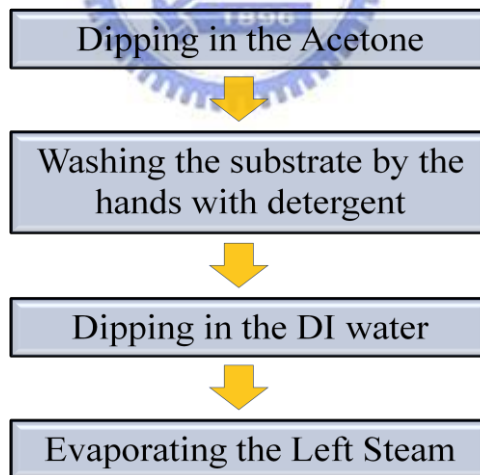


Fig. 3-2 Flow chart of substrate rinsing process

3.1.2 The lithography fabrication process

Lithography technology is adopted to transfer specific patterns from the photomask onto a substrate. The desired patterns were generated by the lithography processes, as

shown in Fig. 3-3. First of all, the spin coater was used to generate the uniform and thin photoresist layer on the surface of the ultra clean glass substrate. A photoresist acts similarly to the sensitizer of a film in a camera since it could optically transfer the patterns of the layout from the photomask. Secondly, the incident UV light beam passes through the photomask which has our designed patterns and reacts with the chemical component of the photoresist. Thirdly, the chemical reacted photoresist can be stripped off and left the no chemical reacted parts. Therefore, our desired patterns are generated on the photoresist after the exposures photoresist is developed. Further, the left photoresist is like a protective layer to its cover ITO part. Therefore, the HCL was used to etch the ITO layer which has no photoresist covered part. Finally, stripping the left photoresist and our designed ITO pattern was generated.

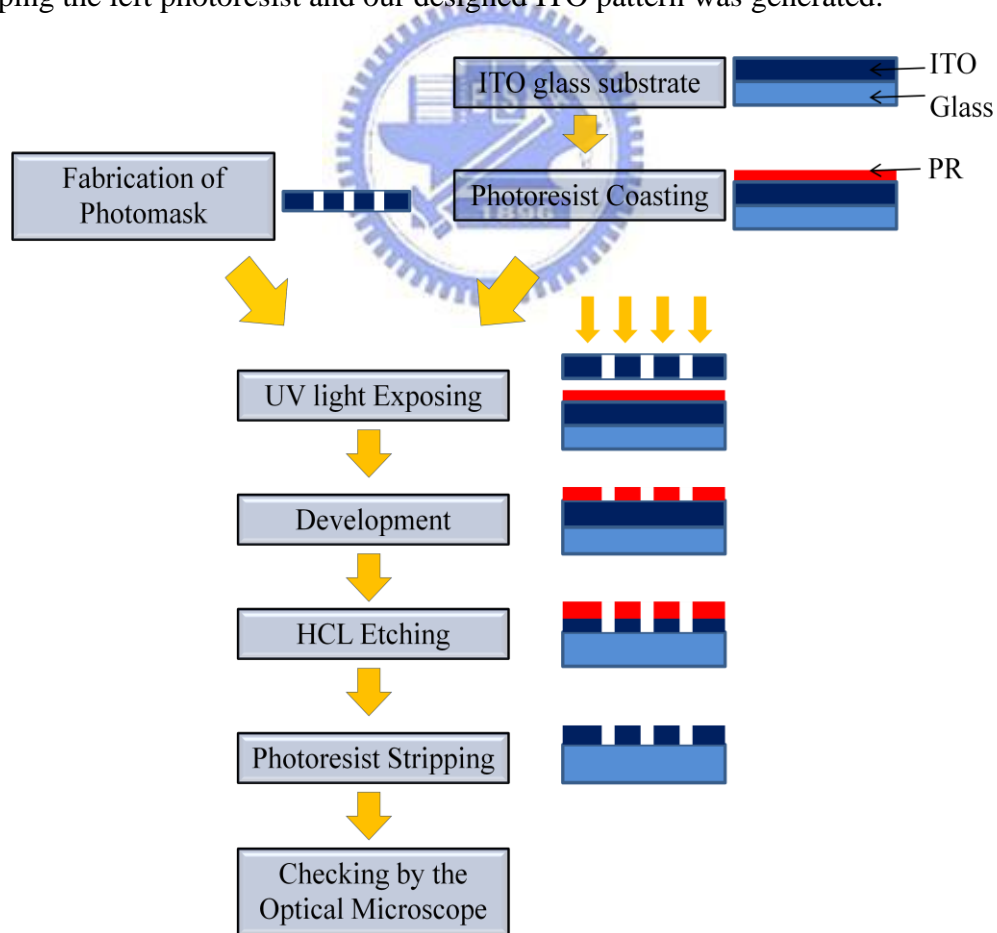


Fig. 3-3 Flow chart of lithography process

3.1.3 The LC device assembly process

This step is used to assemble the whole LC device, and the flow chart of the assembly process is as shown in Fig. 3-4. After the substrates being prepared, the polyimide (PI) is then coated on the substrates to align the LC molecules. Secondly, the roller with woolen texture is used to rub on the PI coated substrate. Thirdly, the spacers are pasted on the substrates to sustain the cell gap, and the top and bottom substrates are assembled which in anti-rubbing direction arrangement. Further, the glue is used to fix and seal one side of the LC cell. Then, the assembled substrates are filled with LC material. Moreover, the glue is used to seal all the seams of the LC cell completely in order to prevent the LC material contact with the air. Finally, the external circuits are connected to the LC device.

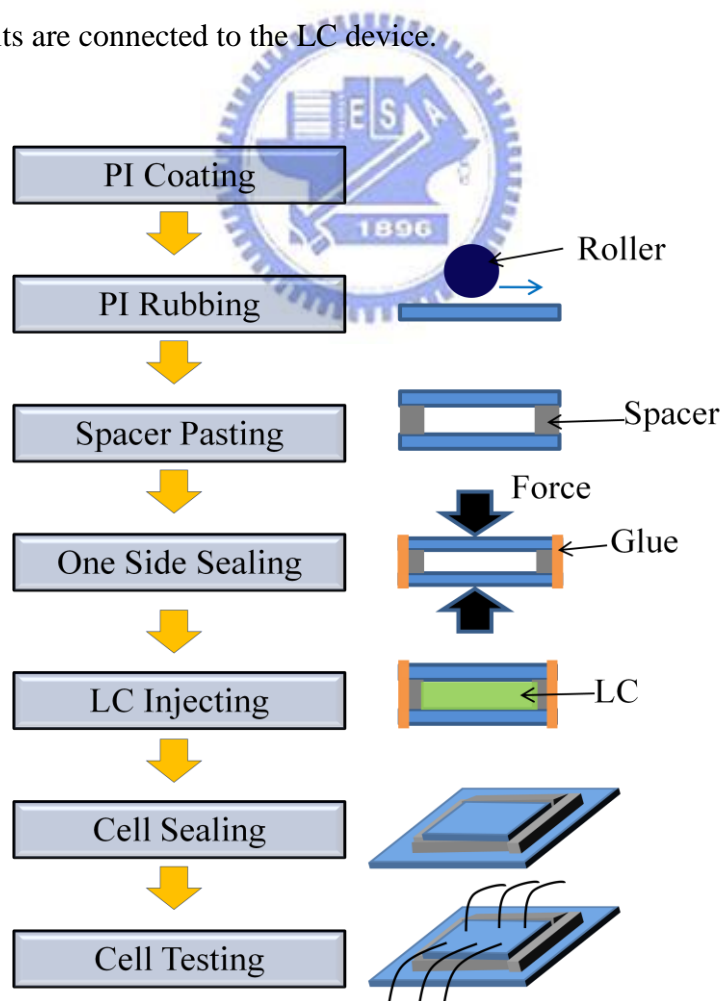


Fig. 3-4 Flow chart of the LC device assembly process

3.2 Measurement System

The measurement system has been constructed, as shown in Fig. 3-5. That consists of laser, beam expander, pin hole, polarizer, our LC lens sample and the beam profile CCD sensor. First of all, the suitable light source from the He-Ne laser will be passed the beam expander to enlarge the beam spot size, pin hole to control the spot size of the passing light beam, polarizer to ensure the certain polarization of passing light beam. Then, the transmitted light beam which has passed the LC lens sample will be measured by the CCD camera. The position with the highest intensity gray level is called the focal length of the LC lens.

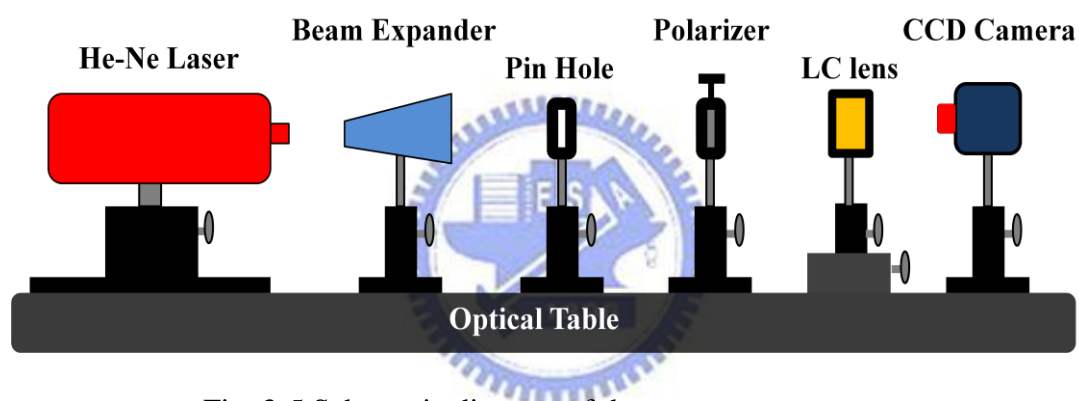


Fig. 3-5 Schematic diagram of the measurement system

3.3 Summary

The fabrication processes are introduced. First, the ITO glass substrates are cut into suitable size and rinsed which is very critical for the following steps. Then, the lithography fabrication processes are used to generate our proposed electrode pattern. Finally, the assembly processes are used to fabricate our proposed LC lens sample. After the LC lens samples were fabricated, the experiment results for the optical performance of LC lens will be measured by the CCD camera. The optical beam profile is as an evaluation criterion and the measurement results will be discussed in chapter 5.

Chapter 4

Simulation Results and Discussions

As mentioned in chapter 2, the LC materials are electrically driven which means the design of electrode pattern is very crucial. Therefore, the simulation model to characterize the feature of the LC lens with electrode pattern has been established. The commercial simulation software 2DiMOS is used to model the LC director and the MATLAB is employed to program the transformation code of the LC director into the refractive index distribution. Based on the principle described in Eq. 2-16, the refractive index distribution of ideal optical lens is a smooth parabolic curve. Therefore, the Error Function has been proposed to calculate the difference between an ideal parabolic curve and the simulation results of LC refractive index distribution to evaluate the focusing ability.

After confirming the refractive index distribution of LC lens, the multi-electrode driven LC lens (MeDLC) has been proposed and the simulation results will be reported in the following.

4.1 Introduction

4.1.1 Simulation software—2DiMOS

The electro-optical calculator Display Modeling System (DIMOS™) developed by Autronic-MELCHERS GmbH was used to simulate the fringing field effect, the graphical user interface is as shown in Fig. 4-1. 2DiMOS calculates the electro-optical properties of LCDs, and allows variations of the molecular orientation in two spatial dimensions so that lateral effects can be taken into account. All three elastic constants

(K_{11} , K_{22} , K_{33}) and the inherent natures are recognized for realistic simulations. The relaxation makes use of the rotational viscosity γ_1 , hence, the dynamics of the director configuration can be revealed. Besides, electrodes, dielectric layer and LC material layer are defined by polygons of arbitrary shape, much like in a standard drawing application. The coupling capacitances of all electrodes can be calculated at arbitrary time levels. A voltage editor is included for the definition of various addressing schemes. Thus, the static and stationary electro-optical response as well as the dynamic behavior can be calculated.

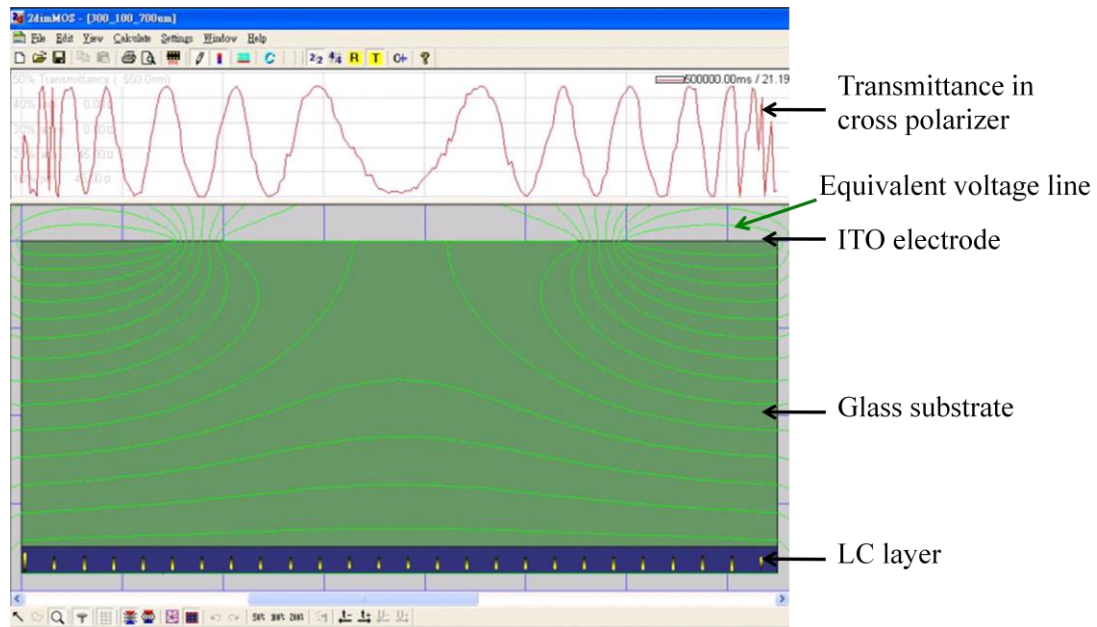


Fig. 4-1 The graphical user interface of 2DiMOS

4.1.2 Evaluation of the lens structure

After editing the initial condition such as the applied voltage and specification of LC material and glass substrate, the LC director can be calculated by the 2DiMOS. These simulation results contain the polar and azimuthal angles of LC director which can be transformed into the refractive index by Eq. 2-11. Therefore, the commercial software MATLAB has been used to program to transform the LC director into

refractive index distribution. Based on Eq. 2-15, since the refractive index difference between the center and edge of the cell (Δn) represent the focal length, the relationship between Δn and radius position can be derived. Based on the principle described in Eq. 2-16, the refractive index distribution of ideal optical lens is a smooth parabolic curve. However, most of the simulation results are not as smooth as the ideal refractive index distribution. Therefore, the Error Function (EF) has been proposed to calculate the difference between the simulation result of LC refractive index distribution and the ideal parabolic curve to evaluate the focusing ability, as described in Eq. 4-1.

$$EF = \sqrt{\frac{\sum_{i=1}^N (S_i - P_i)^2}{N}} \times 100\% \quad (4-1)$$


where N denotes the division number of aperture size, and the S_i and P_i denote the simulation curve value and ideal parabolic curve value, respectively. Since the value of $(S_i - P_i)$ denotes the difference between simulation curve and ideal parabolic curve, to square the value can eliminate the state of plus or minus value which has the same significant. The difference values of every position have been added up to derive the average value which is more objective to evaluate the optical performance of lens structure. The lower EF value represents the simulation result is closer to the ideal optical lens and has higher focusing ability.

4.1.3 Application of our proposed LC lens

As the aforementioned descriptions, our proposed LC lens will be used for camera phone. Therefore, the specification of our proposed LC lens should be similar to the commercial camera phone. Considering the current camera phone lens, the lens aperture is about 1.5mm, as shown in Table 1. This aperture size is also suitable for

our proposed LC lens. After the aperture size has been decided, the most generally used LC material (Merck E7) has been proposed to use in our LC device. The specification of the structure and other simulation parameters are shown in Fig. 4-2 and Table 2.

Table 1. The specification of current camera phone lens

 Ref. Largan Precision Corporation	Composition : 3 Plastic
	F-number : 2.8
	Effective focal length : 4.16mm (paraxial)
	Total thickness length : 5.5mm
	Aperture size : 1.5mm

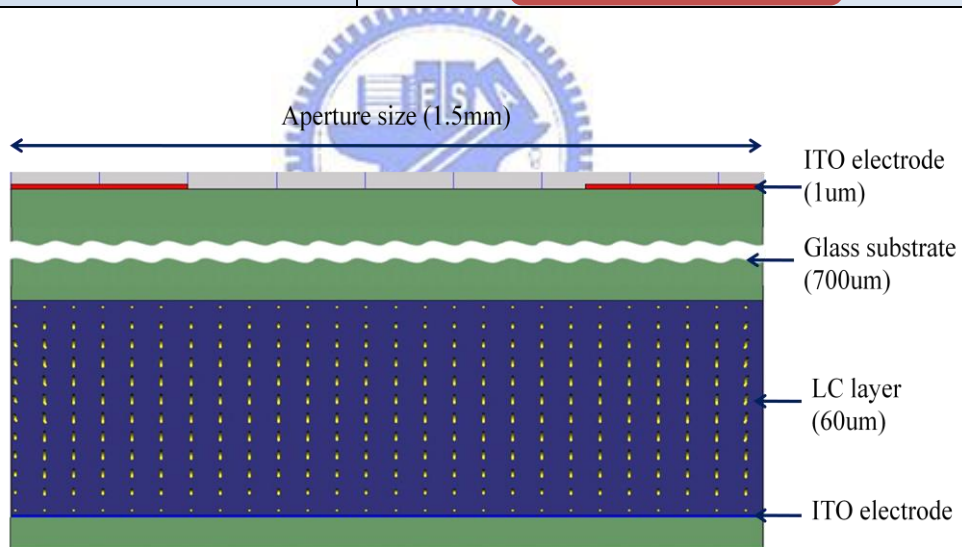


Fig. 4-2 The configuration of our proposed LC lens

Table 2 The parameters for our proposed LC lens.

Items	Specification
Dielectric Constant of Glass Substrate	$\epsilon_{\text{glass}} = 6.9$
The Specification of LC Material (Merck E7)	$K_{11} = 11.1 \text{ pN}$
	$K_{22} = 5.9 \text{ pN}$
	$K_{33} = 17.1 \text{ pN}$
	$\gamma_1 = 233 \text{ m Pa}$
	$\epsilon_{\parallel} = 19.28$
	$\epsilon_{\perp} = 5.21$
	$n_e = 1.7371$
$n_o = 1.5183$	

According to Eq. 2-15, the effective focal length is proportional to the cell gap of LC layer. The thicker cell gap of LC layer has shorter focal length. However, the response time is inverse proportional to the cell gap of LC layer which means the thick cell gap of LC layer has slow response time. The short focal length is traded-off with response time. Therefore, the suitable cell gap of LC layer is 60um and the shortest focal length which can be adjusted is about 4cm.

4.2 ITO electrode pattern design

4.2.1 Simulation results for double-electrode LC lens

After the simulation structure has been set up, the most suitable width of ITO electrode was derived. However, the distribution of Δn is not smooth which means the LC lens has poor focusing ability, as shown in Fig. 4-3. The distribution of Δn curve will become disorder after the applied voltage is increased more than 30 volts

and far away from the ideal smooth parabolic curve. Nevertheless, the distribution of electric field cannot be adjusted due to the low freedom of adjustment in the structure, and the distribution of Δn cannot be improved.

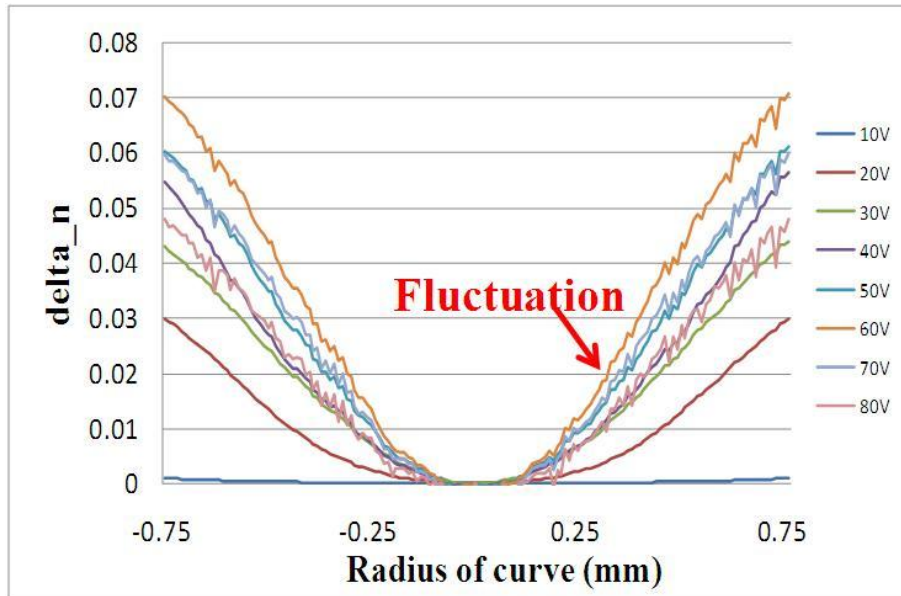


Fig. 4-3 The distribution of Δn of double-electrode structure

Further, the relationship between applied voltage and focal length is not linear, and the maximum Δn value can be acquired at the 60 volts. However, this Δn value is still not large enough which means the focal length is very long. As the applied voltage increased over 60 volts, the maximum Δn value cannot be increased, because the LC director will follow the electric field and almost perpendicular to the electrode plane in the large applied voltage. Therefore, the difference of LC director between the center and edge cannot be varied by increasing applied voltage.

In order to generate a high optical performance LC lens including high focusing ability and short focal length, the multi-electrode driven structure was proposed. Since multi-electrode driven structure has high freedom of adjustment, the refractive index distribution can be adjusted to modify parabolic curve and has large Δn distribution value.

4.2.2 Simulation results of multi-electrode driven structure

The step of finding suitable ITO electrode pattern is as shown in Fig. 4-4. First of all, Δn curve has been fitted with the ideal parabolic curve. We try to find the most suitable electrode number by letting the refractive index to be fixed which means the focal length in the certain value, as shown in Fig. 4-5. The ratio of W_E/W_S has been fixed at 1 at the beginning step, where W_E and W_S denote the electrode width and slit width, respectively. Since a larger Δn value with shorter effective focal length, the largest refractive index ($\Delta n = 0.132$) which can be fitted is used to be the restricted standard. The simulation result shows the most suitable electrode number is 9, as shown in Fig. 4-5.

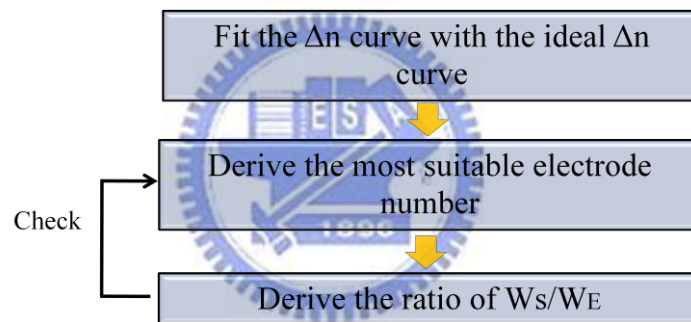


Fig. 4-4 Flow chart of the simulation steps

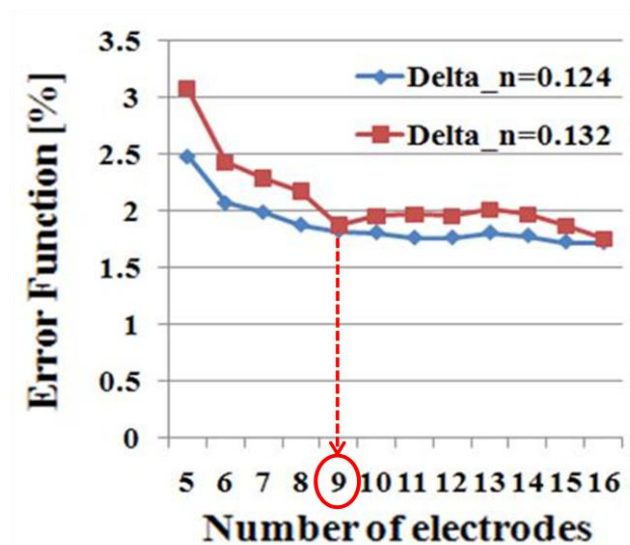


Fig. 4-5 Simulation result of error function with electrode number

As the most suitable electrode number has been derived, the ratio of W_E/W_S was adjusted to derive the lowest EF value, as shown in Fig. 4-6. The simulation result shows the most suitable ratio of W_E/W_S is 1. Therefore, the multi-electrode driven LC lens with 9 electrodes and the ratio of W_E/W_S is 1 where $W_E = W_S = 88\mu\text{m}$ will be used. The simulation result of Δn distribution is as shown in Fig. 4-7. The refractive index curve is very smooth and almost the same to the ideal parabolic curve. Therefore, MeDLC has high focusing ability and large Δn distribution.

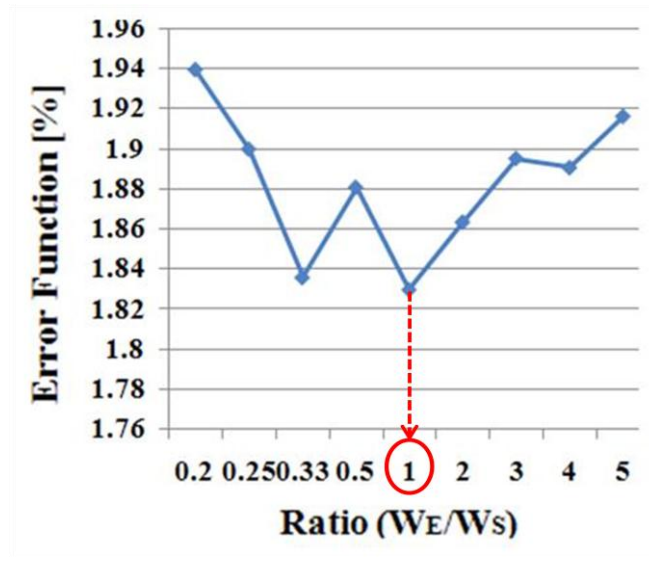


Fig. 4-6 Simulation result of error function with Ratio of W_E/W_S

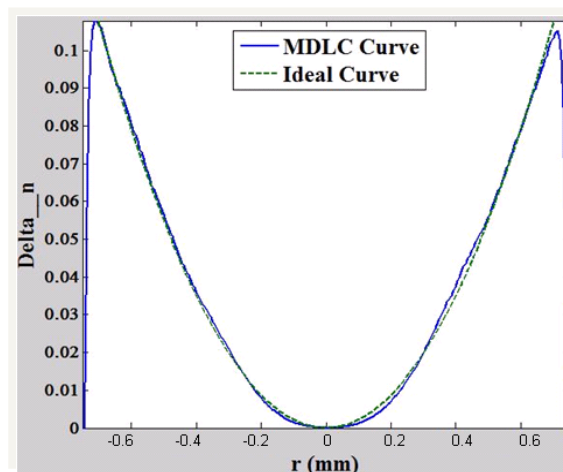


Fig. 4-7 Simulation result of MeDLC structure

4.2.3 Comparison of circular and cylindrical electrode pattern

Most of the references of LC lens discussed about the circular pattern due to it can focus on the incident light by only one LC lens cell. However, the circular electrode pattern is not suitable for multi-electrode structure. The most critical issue of this structure is that the LC director will disorder at the connecting electrode position and generate a poor focusing quality due to the irregular electric field distribution, as shown in Fig. 4-8. This issue is very critical especially in the small size structure. The other method to achieve multi-electrode structure is used multi-ring electrode layers at different layers, as shown in Fig. 4-9. However, this structure is not easy to fabricate.

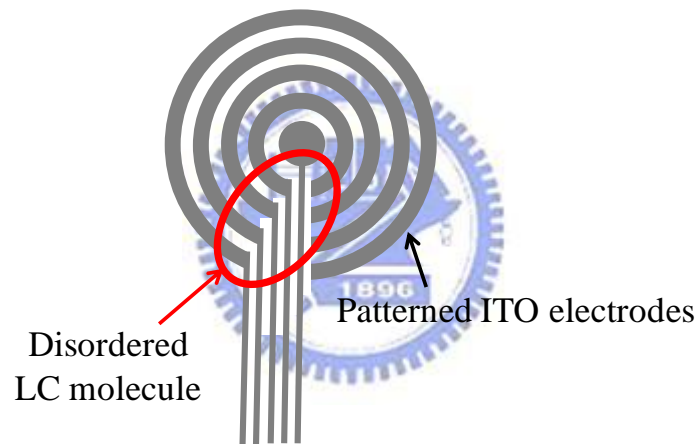


Fig. 4-8 Top view of the multi-electrode circular pattern structure

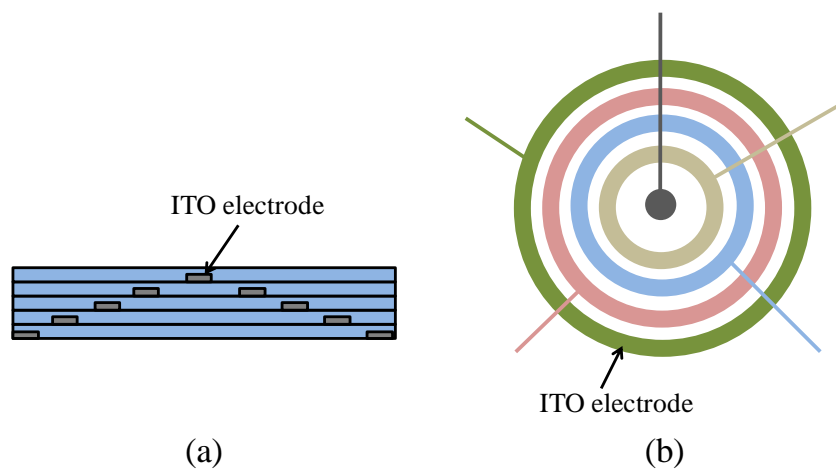


Fig. 4-9 Multi-ring electrode layers structure (a) Side-view and (b) Top-view

In order to overcome these issues, the multi-electrode cylindrical LC lens is used in our application, as shown in Fig. 4-10. This structure does not have the problem of disorder LC molecule at the connecting electrode position and easy to fabricate. To focus on the incident light beam, the half wavelength retarder will be added within the two cylindrical LC lens to change the polarization of the incident light, as shown in Fig. 4-11. The schematic of various polarization conditions are shown in Fig. 4-12. First of all, the incident polarized light beam will be focused into x-direction light line by the LC lens1. Then, the half-wavelength retarder will change the polarization of incident light line into the x-direction where the polarization is parallel to the LC director. Finally, the LC lens2 will focus the x-direction light line into a light point.

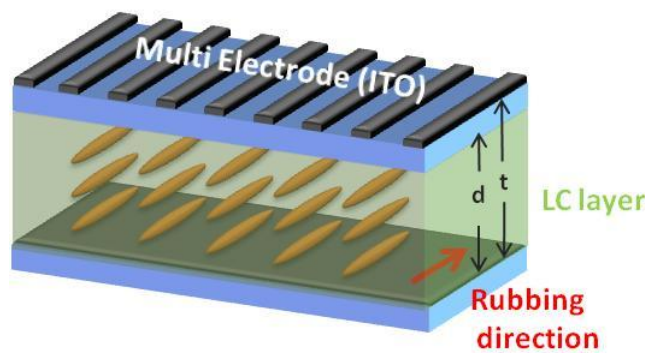


Fig. 4-10 Mechanism of multi-electrode cylindrical LC lens

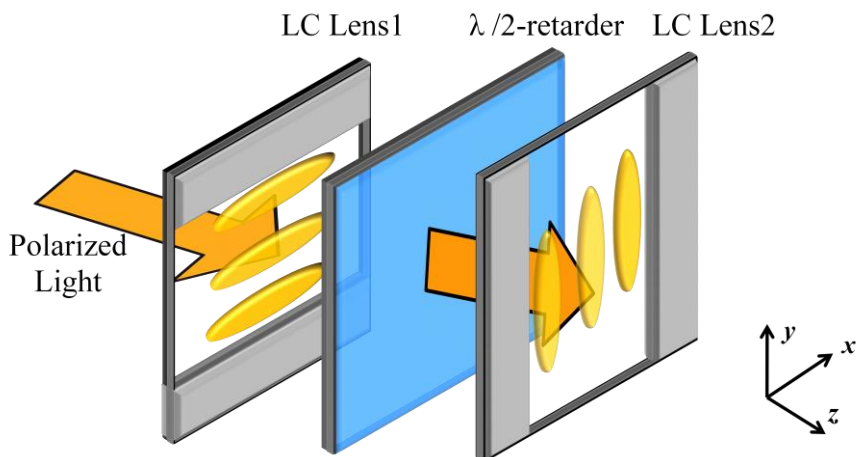


Fig. 4-11 Schematic diagram of the combination of two cylindrical LC lens

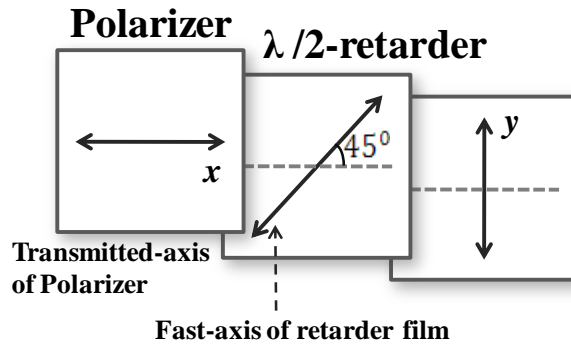


Fig. 4-12 The schematic of various polarizations

4.3 Summary

The LC lens which has smooth gradient refractive index distribution has been designed and the flow chart is shown in Fig. 4-13. The multi-electrode structure has high freedom of adjustment; therefore, it can generate smoother Δn distribution and larger Δn value with shorter effective focal length than the conventional double-electrode structure. Moreover, the multi-electrode structure is not suitable to fabricate in circular shape. Therefore, the multi-electrode cylindrical LC lens with 9 electrodes and the ratio of W_E/W_S is 1 where $W_E = W_S = 88\mu\text{m}$ was used in our application and half-wavelength retarder was used to help the cylindrical LC lens focus on the incident light beam.

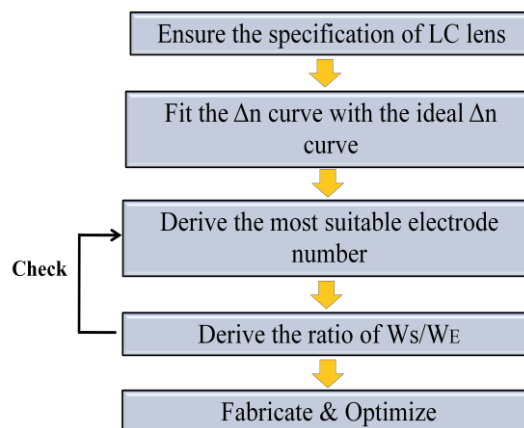


Fig. 4-13 Flow chart of simulation steps for new specification design

Chapter 5

Experimental Results and Discussion

As the ITO electrode pattern has been derived by the simulation, the LC lens device was fabricated accordingly, as shown in Fig. 5-1. In this chapter, the experiment results of focusing ability between multi-electrode driven cylindrical LC lens (MeDLC) and 2-electrode structure will be compared. Additionally, the other issue in MeDLC is the slow response time which is very critical for our application. Therefore, we proposed to apply large applied voltage on the electrodes in a short time interval to help the LC orientation and reduce the response time.



Fig. 5-1 The multi-electrode driven cylindrical LC lens sample (MeDLC)

5.1 Experiment results for focusing ability

In order to evaluate the focusing ability of LC lens, we consider the full width at half maximum method (FWHM) to compare different beam profiles. The FWHM value is given by the distance between points on the curve at which the function reaches half of its maximum value. This method is well-defined number which can be used to compare the focusing performance obtained under different observing conditions and better reflect the approximated size of the beam profile. The smaller FWHM value implies the better focusing performance which can generate sharp

image.

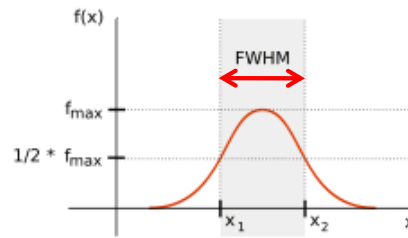


Fig. 5-2 The diagram of FWHM

5.1.1 Comparison of MeDLC and double-electrode cylindrical lens

The MeDLC has high freedom to adjust the voltages to modify the distribution of refractive index and generate smoother gradient refractive index distribution than the double-electrode structure. The experimental results with fixing focal length at 4cm which is the shortest focal length are shown in Fig. 5-3. The FWHM values of MeDLC and double-electrode structures are 0.047 and 0.084 mm, respectively. The FWHM value of MeDLC was improved by 44%.

On the other hand, since the MeDLC has high freedom of adjustment, the distribution of refractive index can be modified to large Δn value with smaller applied voltage. When the focal length has been fixed at 4cm, the applied voltages in MeDLC and double-electrode structure are 34volts and 60volts, respectively. The MeDLC can achieve shorter focal length by applying smaller applied voltage than the double-electrode structure.

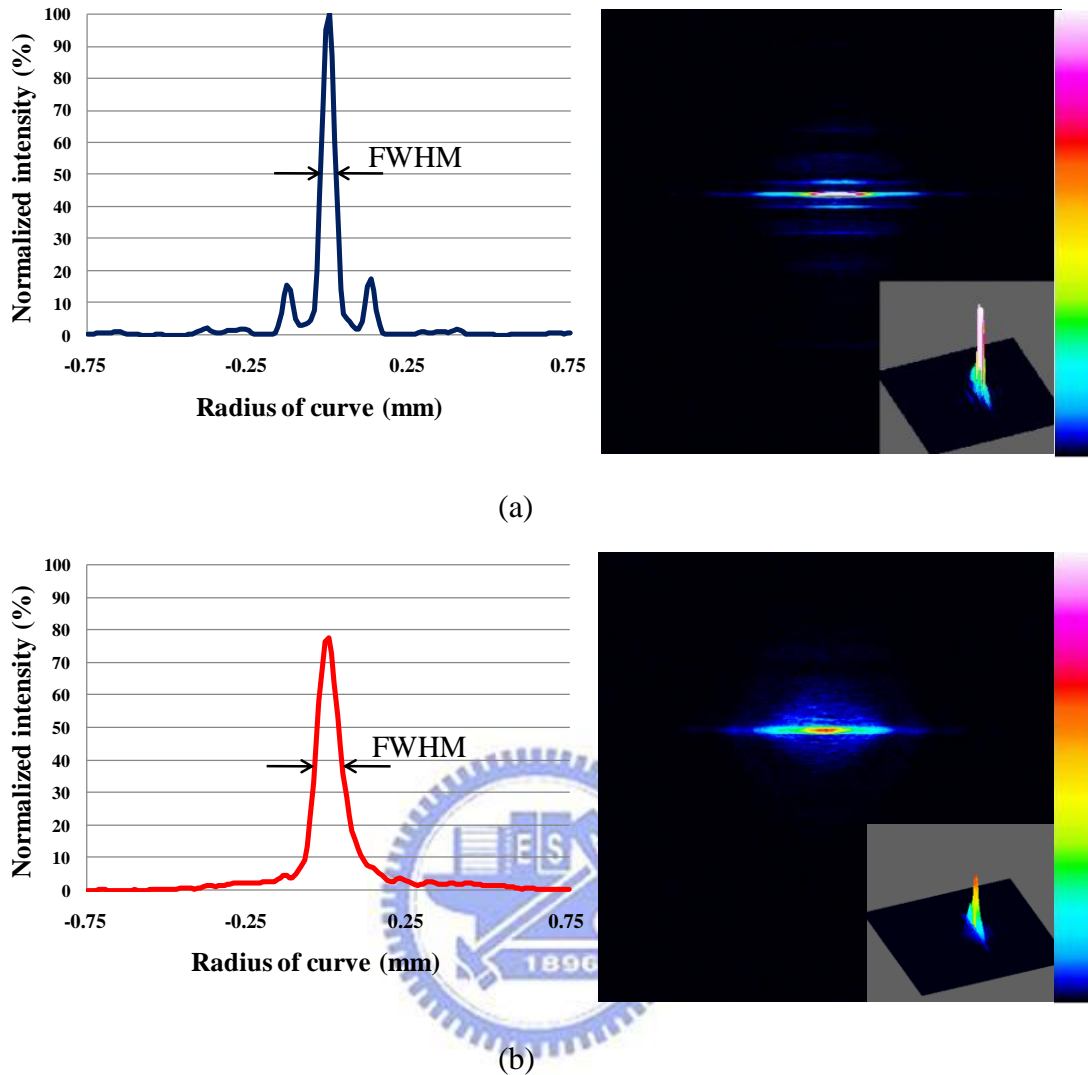


Fig. 5-3 Experiment results for distribution of intensity which the focal length was fixed at 4cm : (a) MeDLC and (b) double-electrode cylindrical structure

The distribution of intensity on MeDLC has two minus peak value at about $\pm 0.2\text{mm}$ position due to the diffraction effect; the light source in our experiment is He-Ne laser which has long coherent length, as shown in Fig. 5-3(a). As the incident light passing by the electrode layer, the diffraction effect was generated by the electrode pattern. However, in the application of camera phone, the diffraction effect will not generate in the real image due to the daylight lamp has short coherent length.

5.1.2 Comparison of two combined MeDLC and single circular electrode structure lens

Since the MeDLC has smaller beam size than the double-electrode structure lens, two MeDLC lenses were combined in cross direction to focus on the incident light beam. The experiment system of combined MeDLC lens is shown in Fig. 5-4. Here, we compared the focusing performance of single circular electrode structure with combined MeDLC lens by fixing the focal length at 4cm, and the experiment results are shown in Fig. 5-5.

The FWHM values of single circular electrode structure and combined MeDLC are 0.23 and 0.05mm, respectively. The FWHM value of combined MeDLC was improved by 78%. The combined MeDLC lens can effectively focus on the polarized incident light beam into a light spot, and the beam size is smaller than the single circular electrode structure.

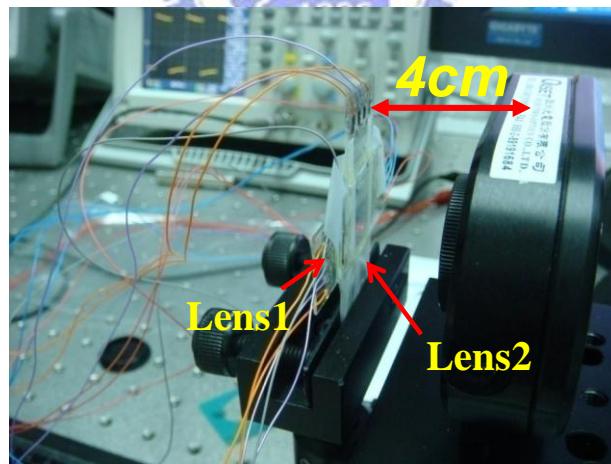


Fig. 5-4 Photo of experimental system of combined MeDLC

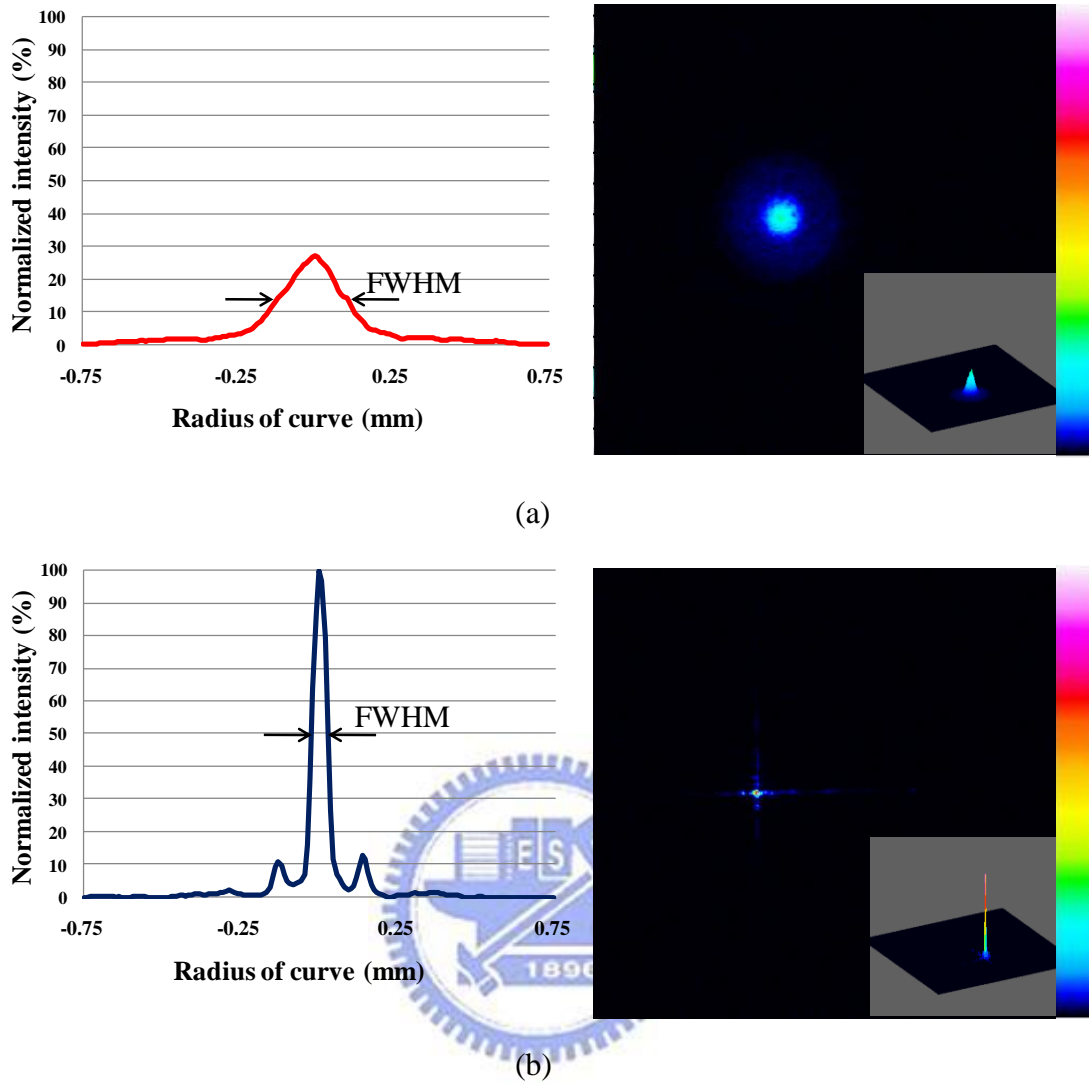


Fig. 5-5 Experimental results for distribution of intensity :

(a) Single circular electrode structure and (b) combined MeDLC

5.1.3 Combined MeDLC was used in image system

After measuring the beam profile of combined MeDLC, the combined MeDLC was used in image system. The FPGA hardware was used to take photograph, and the experimental results are shown in Fig. 5-6. However, although the combined MeDLC has small beam size, the image quality is not good enough.

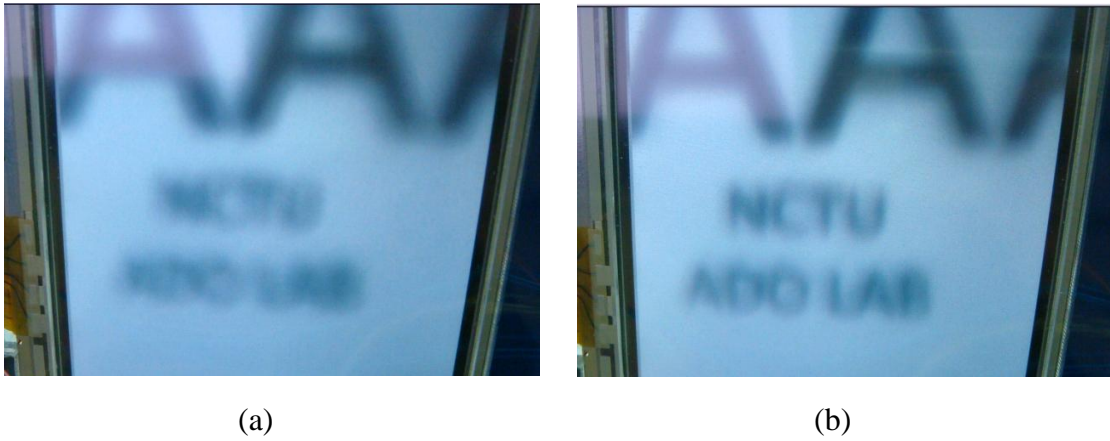


Fig. 5-6 The image results in FPGA : (a) LC lens without applied voltage
and (b) LC lens with applied voltage

The poor image quality may due to three issues. The first issue is the structure of combined MeDLC. The thickness of half-wavelength retarder will affect the incident light beam when the incident light beam was not parallel to the optical axis, as shown in Fig. 5-7. Therefore, the combined MeDLC does generate serious optical aberration.

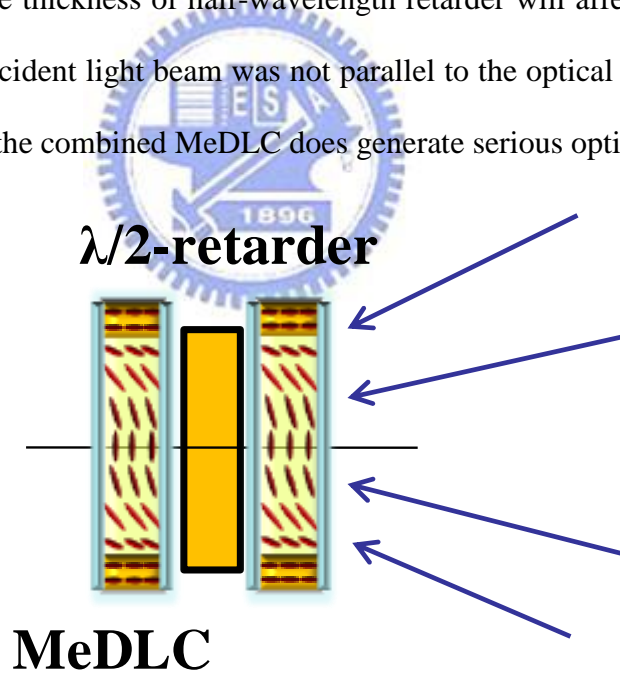


Fig. 5-7 The combined MeDLC may generate serious optical aberration

The second issue is due to the distribution of intensity on MeDLC has two minus peak value, as shown in Fig. 5-3. In order to ensure the effect degree of the two minus peak value, we simulate the modulation transfer function (MTF) to describe the

performance of a lens system, as shown in Fig. 5-8. The calculating function can be described in Eq. 5-1. This method has been widely used in the evaluation of lens quality [15].

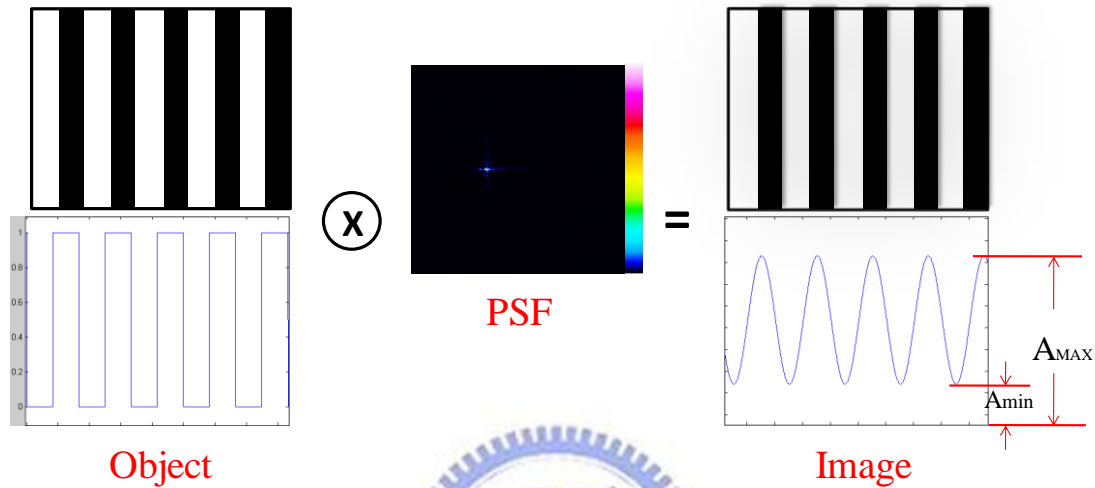
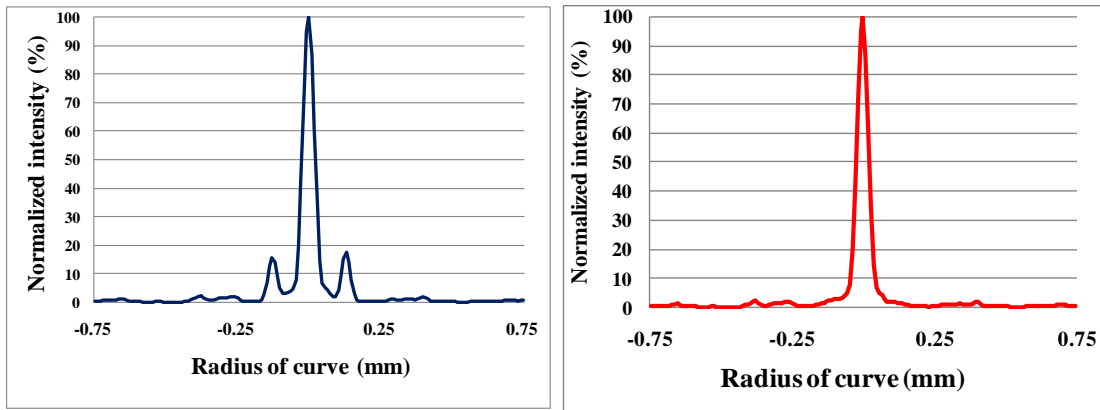


Fig. 5-8 The calculation of MTF by convoluting the rectangle wave and beam profile

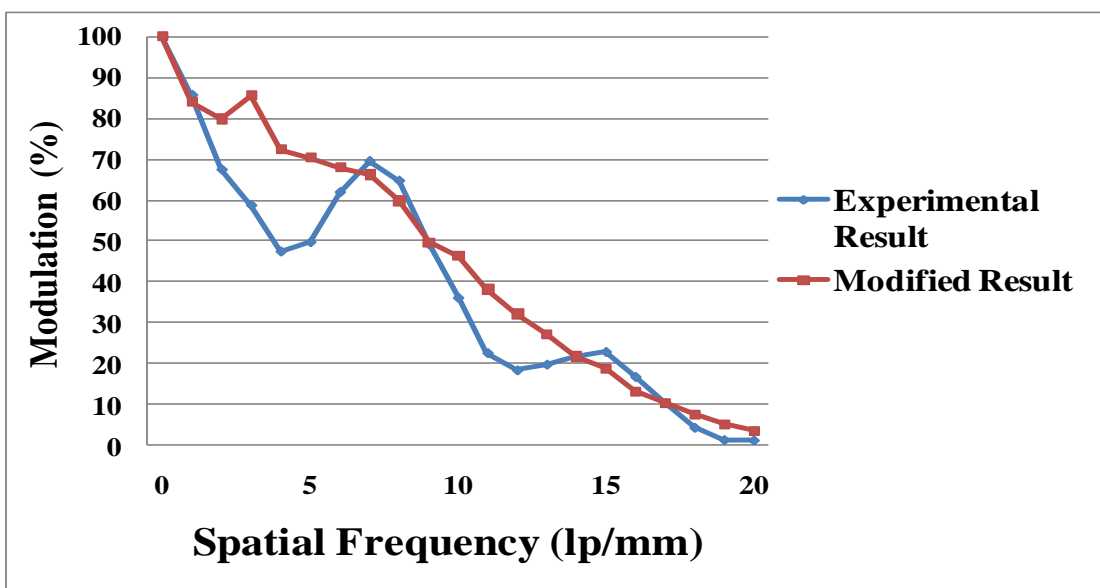
$$MTF = \frac{A_{Max} - A_{min}}{A_{Max} + A_{min}} \quad (5-1)$$

where A_{Max} and A_{min} are the maximum and minimum image illumination levels, respectively. The comparison of experimental result and modified result are shown in Fig. 5-9. The modified result of beam profile has removed the distribution of two minus intensity. Since the MTF of modified beam profile has better optical performance, the two minus peak value have serious effect. Therefore, we should adjust the LC lens structure which will not generate the distribution of two minus intensity.



(a)

(b)



(c)

Fig. 5-9 The calculating results of MTF by the beam profile : (a) the experimental result of beam profile, (b) the modified result of beam profile and(c) the comparison of MTF in different beam profile

The third issue which may contribute poor image quality is the optical system. The present optical system may not suitable for the MeDLC. This issue is very critical especially when the lens has large optical power. Therefore, the optical system in our experimental setup should be redesigned to reduce the optical aberration. The optical system can be simulated by the simulation software such as light tool and OSLO to

find the most suitable optical system.

The first and second issues will be solved by our proposed dot array structure which will be described in chapter 6.

5.2 Experimental results for response time

The response time of LC lens is very critical for our application. Refer to the reference; the response time (t_{rise}) of the LC lens is defined as the time elapsed after the application of the voltages to reach to the 90% of the saturated intensity value.[16] This method is well-defined number which can be used to compare the response time obtained under different observing conditions. Therefore, the method was used in this thesis.

5.2.1 Over-driving method: giving large applied voltage for a short time interval to help LC molecule orientation

Although a thicker LC layer can lead to a shorter focal length, the thick LC cell gap is traded-off with slow response time. According to Eq. 2-9, the response time is proportional to the square of cell gap (d^2). Moreover, the LC response time is inversely proportional to applied voltage square (V^2). Although the MeDLC can be driven by a smaller applied voltage to achieve shorter focal length, the response time is traded-off with applied voltage.

The response time of MeDLC is about 17 seconds which is very slow for our application, as show in Fig. 5-10.

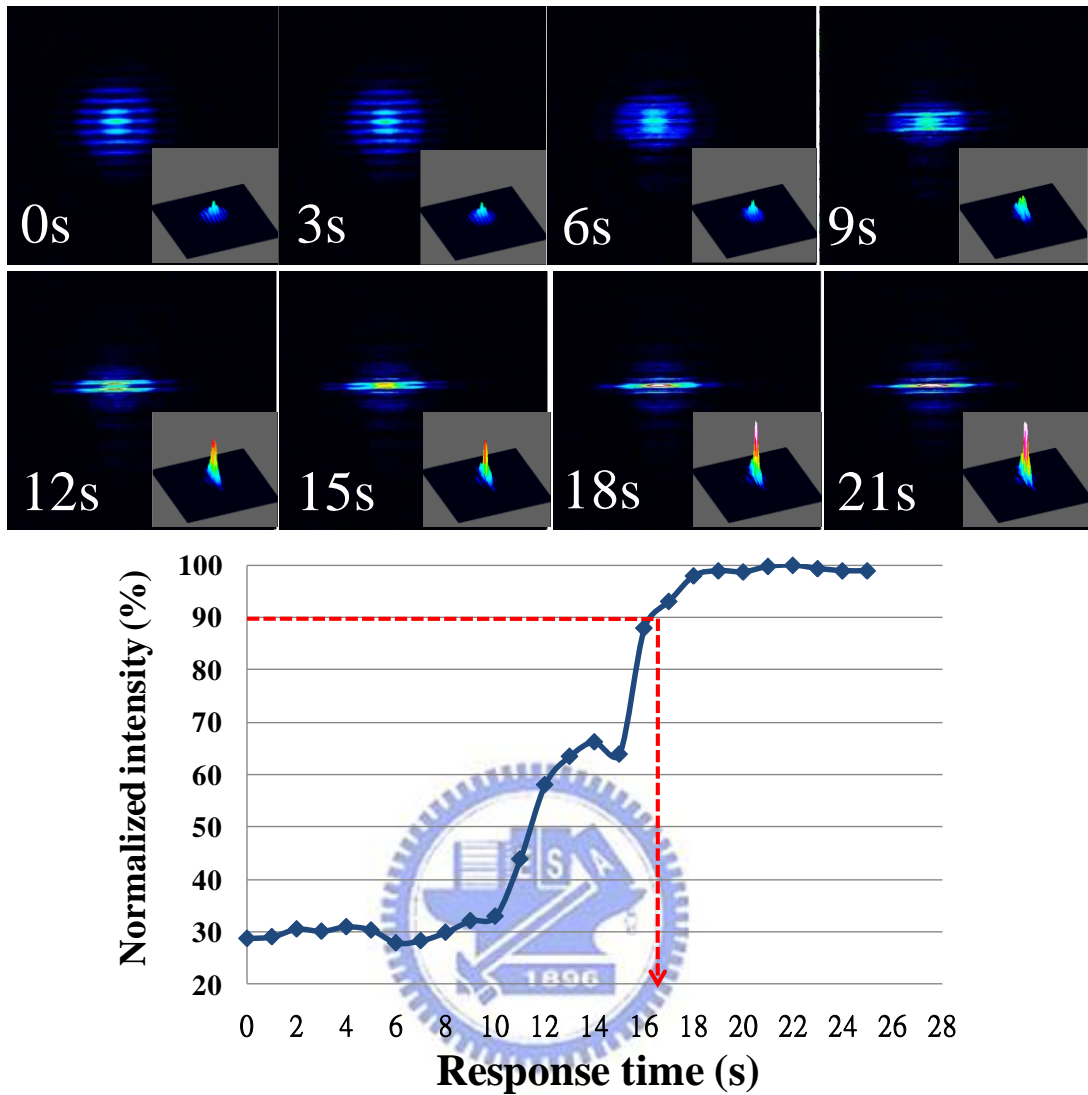


Fig. 5-10 Experimental results of MeDLC on intensity value as a function of time

In order to overcome this issue, we propose to apply large applied voltage in a short time interval to speed up the initial LC molecules at the beginning, which called over-driving method. Therefore, the initialized response time of LC lens can be reduced. However, the area of each electrode of MeDLC is too small to drive the whole LC molecule. Therefore, two larger electrodes were proposed to add outside the original 9 electrodes of MeDLC, as shown in Fig. 5-11. Before applying the desired applied voltage on the inner 9 electrodes (V_M), we first apply large applied voltage on the outer large electrodes (V_L) in a short period of time (Δt). The method of applying

voltages is shown in Fig. 5-12.

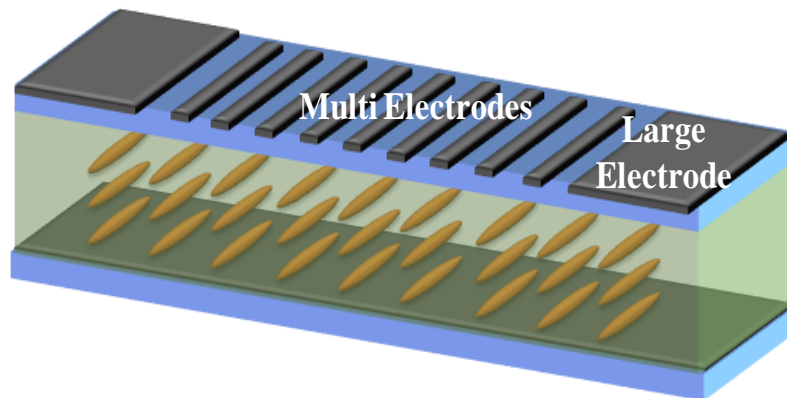


Fig. 5-11 Two larger electrodes were added outside the original 9 electrodes

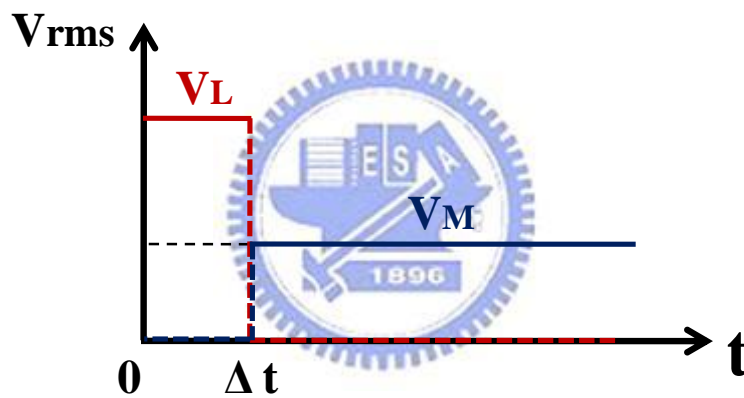


Fig. 5-12 The voltage control system in over-driving method

As applying large applied voltage on the outer large two electrodes, the LC lens has reached the 90% of the saturated intensity value in a short period of time (Δt). Several different V_L values were applied for the focal length at 4cm and the result is shown in Fig. 5-13. The experimental result for applied voltage on 80Vrms of intensity value as a function of time is shown in Fig. 5-14. However, when V_L value larger than 80 Vrms, the LC molecule was over-driving and distribution of refractive index will need a little time to vary from flat bottom curve and to parabolic curve, as shown in Fig. 5-15.

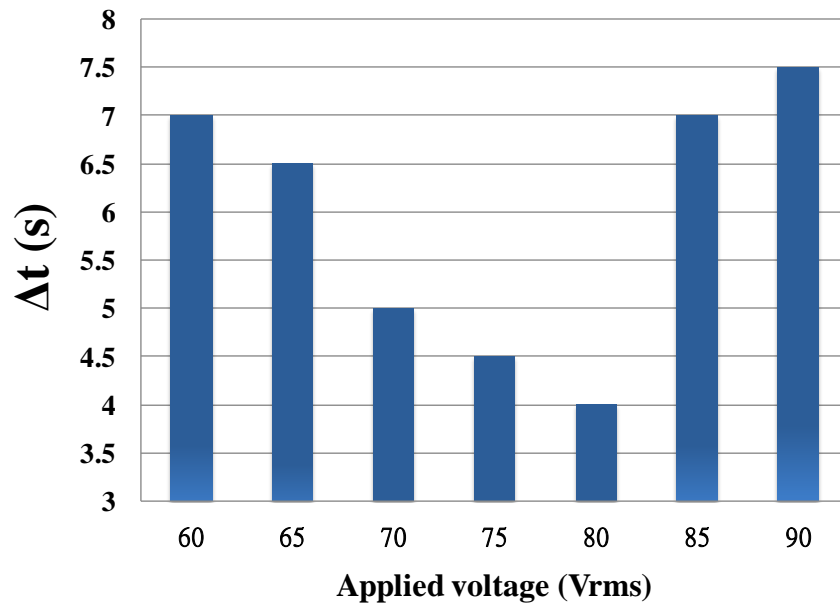


Fig. 5-13 Experimental result for the Δt with different applied voltage of the outer large electrodes (V_L)

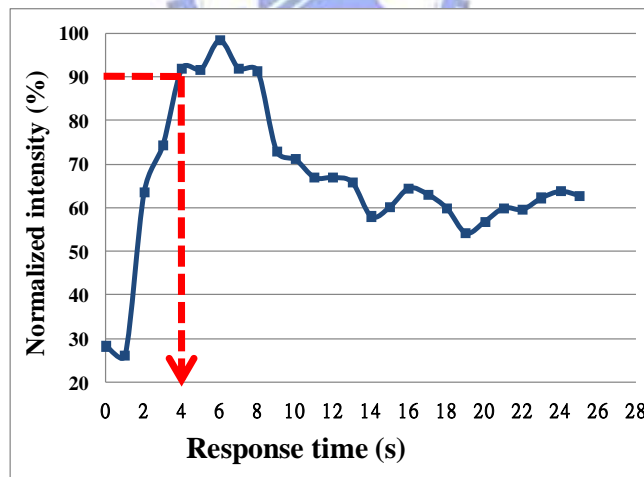


Fig. 5-14 The experimental result for the applied voltage on 80Vrms of intensity value as a function of time

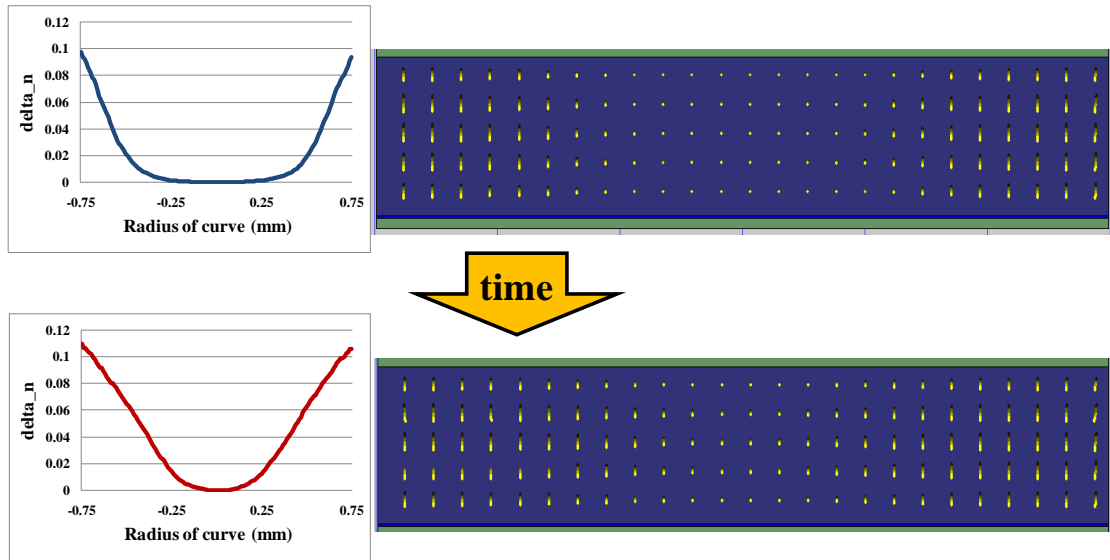
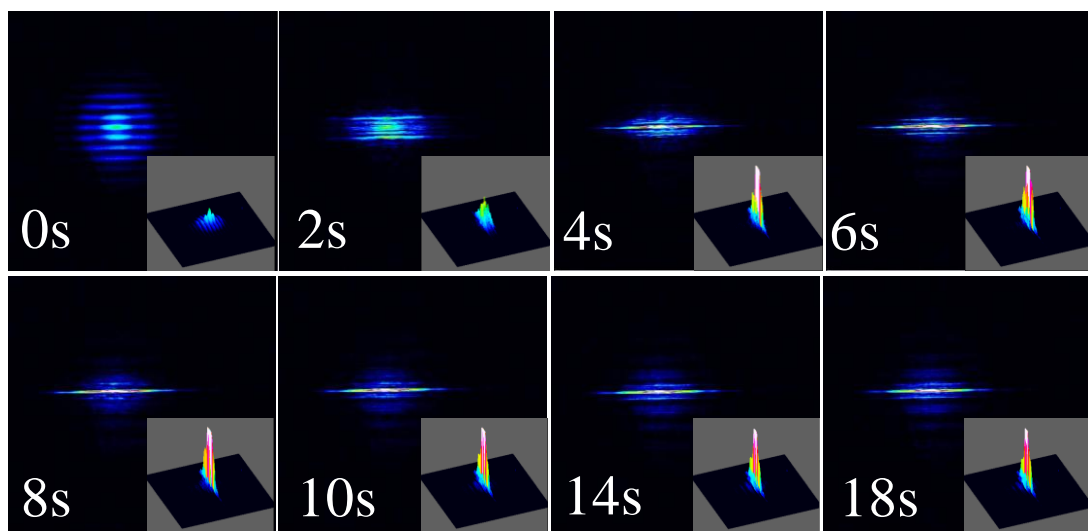
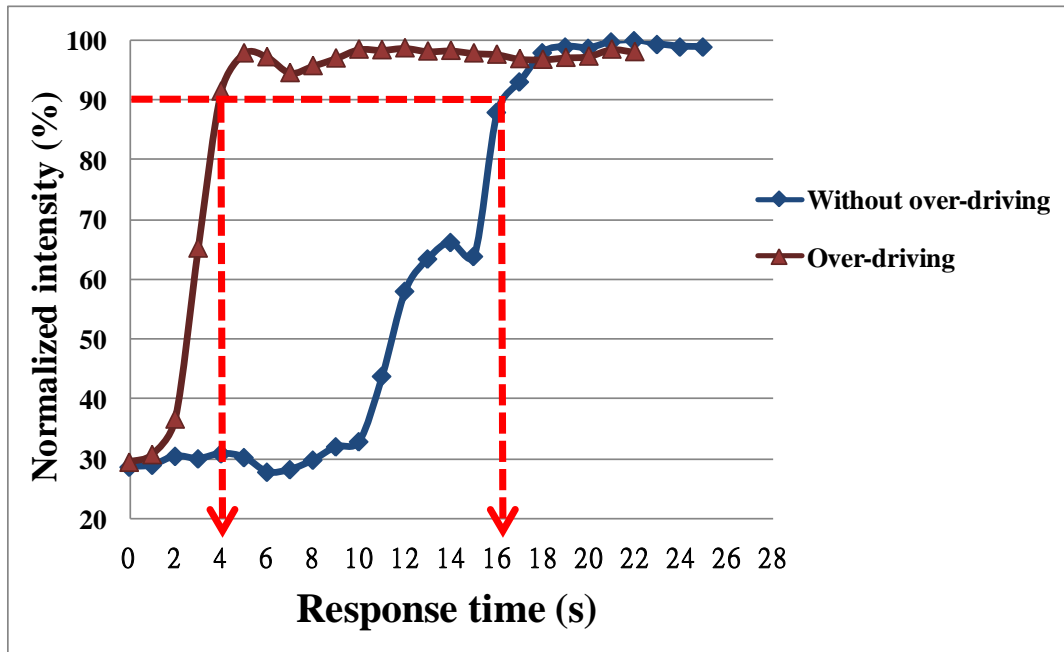


Fig. 5-15 Too large applied voltage will induce large Δt value

Therefore, V_L value on 80 Vrms which has the shortest time interval ($\Delta t=4s$) was used to improve the response time of MeDLC and the results are shown in Fig. 5-16. The LC molecule can orient quickly at the beginning of focusing and reduce the initial response time. The response time was reduced from 17 seconds to 4 seconds, improved by 3.25 times. Therefore, giving large applied voltage on the outer large electrodes (V_L) can help the LC molecule orientation and reduce the response time of LC lens.



(a)



(b)

Fig. 5-16 The experimental results for distribution of intensity at $V_L=80V_{rms}$ and $\Delta t=4s$, (a) distribution of intensity gray level and (b) intensity value as a function of time



5.3 Summary

The FWHM was used to evaluate the focusing performance. The FWHM value of MeDLC and combined MeDLC were improved by 44% and 77%, respectively, because the multi-electrode structure has high freedom of adjustment to modify the distribution of refractive index. Moreover, in order to improve the response time, large applied voltage was given to the outer large 2 electrodes ($V_L=80V_{rms}$) for a short time interval ($\Delta t=4$ seconds) to help LC molecule orientation. The experimental result shows that the response time was improved by 70%. Therefore, the multi-electrode cylindrical LC lens is more suitable than double-electrode structure for the application of camera phone.

Chapter 6

Conclusions and Future work

6.1 Conclusions

The tunable lens has been widely used for the optical system and other electro-optic devices. The conventional tunable lenses need moving mechanical space to adjust the focal length. However, the LC lens is electrically tunable and no moving mechanical part. Therefore, the LC lens can smaller and lighter than the conventional tunable lenses and these advantages are very critical especially in the compact volume application.

In order to generate high focusing performance LC lens, we compared the double-electrode with multi-electrode structure by the simulation of proposed 9 electrodes with $W_E/W_S=1$ in cylindrical structure. The experimental result shows the FWHM value of MeDLC was improved by 44%. Additionally, two MeDLC cylindrical lenses were combined to focus on the incident light beam. The experimental result shows the FWHM of 2-crossed MeDLC was improved by 77%. To speed up response time, we added two large electrodes outer the original 9 electrodes and applied large applied voltage for a short period of time to speed up the initial LC molecule orientation. The response time was improved by 3.25X.

In conclusion, the multi-electrode structure has more freedom to control the LC molecule to generate better focusing performance. Moreover, the response time of LC lens can be improved by controlling the applied voltage to speed up the initial LC molecule. Therefore, the MeDLC is more suitable than conventional double-electrode structure for the application of camera phone.

6.2 Future work

The proposed multi-electrode driven cylindrical LC lens has been demonstrated to improve the focusing performance with smaller applied voltage (~34volts). However, the response time has also improved by applying large applied voltage for a short period of time method (~5seconds). However, the applied voltage and response time are still unacceptable. Therefore, we propose to combine electrode layer with high resistance material to generate gradient voltage distribution [17]. The high resistance layer does help the electrode layer to generate gradient voltage distribution. However, the high resistance layer has a limited effect in double-electrode structure, and the distribution of electric field cannot smooth enough to generate gradient refractive index distribution. Therefore, this method must combine with multi-electrode structure which is high freedom of adjustment, as shown in Fig. 6-1.

However, combining the cylindrical electrodes with high resistance material directly cannot help to generate gradient distribution of potential. The distribution of potential will have the same value in each area of the electrode and the LC layer cannot have a gradient refractive index distribution. The cylindrical structure will induce rectangle equivalent voltage line, as shown in Fig. 6-2. To overcome this issue, we propose to use dot array electrodes with high R material instead of cylindrical electrodes structure, as shown in Fig. 6-3. The dot array structure can generate lens-like gradient distribution of potential between the electrodes. Therefore, the dot array structure has no issues of combined MeDLC and minus peak intensity value. Moreover, the LC lens with dot array electrodes has higher degree of freedom in adjustment reaching better focusing performance.

Nevertheless, combining the electrodes with high resistance material may yield the thermal issue. The high resistance material will generate thermal energy while

applying the applied voltage on the electrodes. However, since the electrodes can be placed inside the glass substrate, the applied voltage can be reduced under 10 volts. Therefore, the effect of power generated by high resistance material may not serious, and the level of effect has to be further studied.

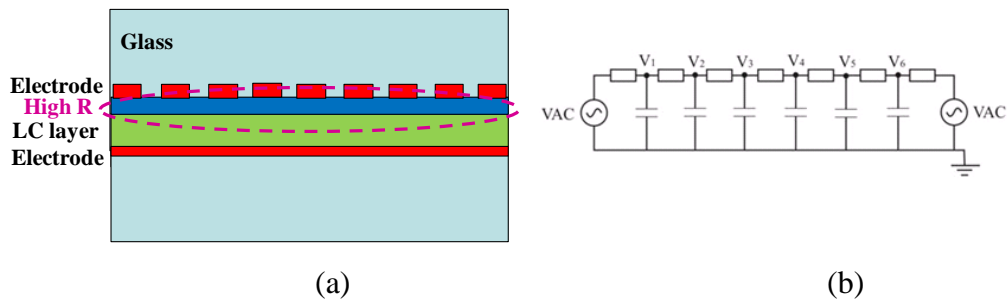


Fig. 6-1 The concept of combining electrodes with high resistance layer, (a) side-view and (b) equivalent circuit of high resistance layer

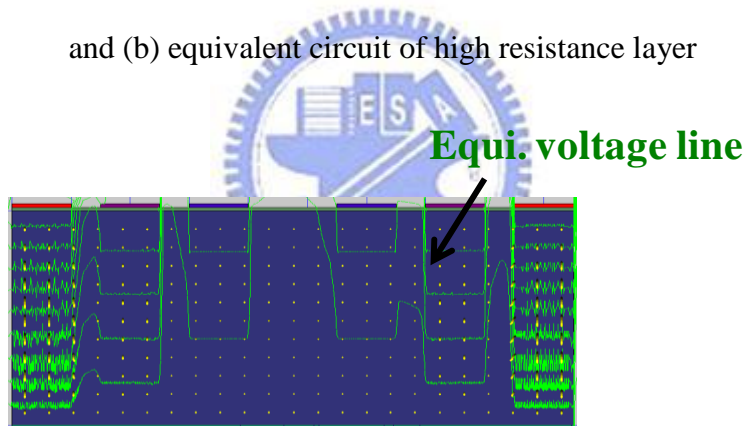


Fig. 6-2 Cylindrical structure will induce rectangle equivalent voltage line.

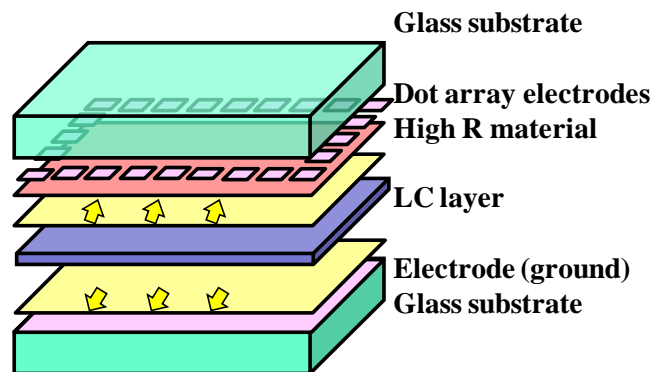


Fig. 6-3 The schematic of dot array electrodes with high R material structure

References

- [1] Eugene Hecht, OPTICS, Addison Wesley (2002)
- [2] H. Ren. and S. T. Wu, Variable-focus liquid lens, Opt. Express. 15, 10, pp. 5931 (2007)
- [3] Varioptic, The Liquid Lens company, <http://www.varioptic.com/en/index.php>
- [4] S. Sato, Liquid-crystal lens-cells with variable focal length, J. J. Appl. Phys, 18, pp. 1679 (1979)
- [5] H. Ren, Y. H. Lin, and S. T. Wu, Adaptive lens using liquid crystal concentration redistribution, Appl. Phys. Lett., 88, 19 (2006)
- [6] P. E. Cladis and S. Torza, Stability of Nematic Liquid Crystals in Couette Flow, Phys. Rev. Lett. 35, pp. 1283 (1975)
- [7] H. C. Tseng, Dayton L. Silver, and Bruce A. Finlayson, Application of the continuum theory to nematic liquid crystals, Phys. Fluids 15, pp. 1213 (1972)
- [8] D.W. Berreman, Optics in Stratified and Anisotropic Media, J. Chem. Phys. 62, pp. 776 (1975)
- [9] D. K. Yang, S. T. Wu, Fundamentals of Liquid crystal devices (2006)
- [10] A. Muravsky, A. Murauski, V. Mazaeva, V. Belyaev, Parameters on the LC alignment of organosilicon compound films, J. Soc. Inf. Disp. 13, pp. 349 (2005)
- [11] H. Gruler and L. Chang, Dielectric Alignment in an Electrically Conducting Nematic Liquid Crystal, J. Appl. Phys. 46, pp. 5097 (1975)
- [12] J. Nehring, A. R. Kmetz, and T. J Scheffer, Analysis of weak-boundary-coupling effects in liquid-crystal displays, J. Appl. Phys. 47, pp. 850 (1976)

- [13] E. Jakeman and E. P. Raynes, Electro-optics response times of liquid crystal, Phys. Lett. A39, pp. 69 (1972)
- [14] I. C. Khoo and S. T. Wu, Optics and Nonlinear Optics of Liquid Crystals, World Scientific, Singapore (1993)
- [15] J. W. Goodman, Introduction to Fourier Optics, New York: McGraw-Hill (2005)
- [16] M. Ye, S. Sato, New Method of Voltage Application for Improving Response Time of a Liquid Crystal Lens, Mol. Cryst. Liq. Cryst., 433, pp. 229 (2005)
- [17] A. F. Naumov and M. Yu. Loktev, Liquid-crystal adaptive lenses with modal control, Opt. Lett., 23, 13, pp. 992 (1998)

